Journal of Asian Earth Sciences 255 (2023) 105780

Contents lists available at ScienceDirect

Journal of Asian Earth Sciences

journal homepage: www.elsevier.com/locate/jseaes

Constraints of C–O–Sr isotope and elemental geochemistry on the origin of dolomite of the deeply buried Ediacaran sedimentary succession, central Sichuan Basin (SW China)

Yishu Li [a,b], Guangdi Liu [a,b,*], Zezhang Song [a,b], Mingliang Sun [a,b], Xingwang Tian [c], Dailing Yang [c], Yunlong Wang [c], Lianqiang Zhu [a,b], Fuliang You [a,b]

[a] State Key Laboratory of Petroleum Resources and Prospecting, China University of Petroleum, Beijing 102249, China
[b] College of Geosciences, China University of Petroleum, Beijing 102249, China
[c] Exploration and Development Research Institute of Southwest Oil & Gas Field Company, PetroChina, Chengdu 610041, China

ARTICLE INFO

Keywords:
Mineral stage
Dolomitization
LA-ICP-MS elements
C–O–Sr isotope
Rare earth elements
Ediacaran

ABSTRACT

It is significant and challenging to study the formation mechanism of multistage dolomite and the characterization of various fluid alteration in multi-tectonic cycles, ancient, and deeply-ultra-deeply buried carbonate rocks. The Sichuan Basin is a superimposed multicycle basin with abundant oil and gas resources and complex geological evolution, in which there are multiple dolomite textures in the Ediacaran sedimentary succession (~542 Ma) and the burial depth is more than 7000 m in geological history. Therefore, this study combines petrology, C–O–Sr isotope, ordering degree, fluid inclusions, and elemental geochemistry methods to systematically restore the mineral stages and identify the fluid information to analyze the origin of multistage dolomite. The results show that the host rock → dolomite-1 → bitumen-1 → dolomite-2 → bitumen-2 → quartz, accompanied by some metal minerals dominate the Ediacaran Dengying Formation. After normalization by seawater value, the light rare earth elements (REE) were enriched while the heavy REE were depleted in all dolomites. The results also show that the joint analysis of isotopes and elements is reliable under deep burial conditions, whereas the ordering degree needs to be treated with caution as the potential irregularity increases with burial depth or evolution to a certain extent. Dolomite-2 has more negative C–O isotope and higher Sr isotope than Precambrian seawater and Eu anomalies, indicating the origin of formation water and deep thermal fluids during its burial dolomitization. The formation of the host rock is the joint result of microbial action, evaporation, and backflow infiltration under seawater conditions. It is dominated by mud crystals, retaining some primary structures. Dolomite-1 was formed between the host rock and dolomite-2, which is the product of shallow burial and the fluid is a mixture of seawater and basinal brine.

1. Introduction

With the increasing demand for fossil energy and the rapid development of oil and gas exploration engineering technology, the current hydrocarbon exploration work is gradually moving toward deep, ultra-deep, and ancient strata (Dyman et al., 2002, 2003; Sun et al., 2013; Luemba et al., 2021; Ma et al., 2022; Wang et al., 2022). Furthermore, oil and gas in carbonate rocks account for more than 60% of the total resources globally, such as in North America, the Middle East, and Central Asia (Bagrintseva, 2015; Li et al., 2018). The Precambrian–Cambrian system is a critical period in the global environment and ecosystem evolution (Hoffman, 1998; Kimura and Watanabe, 2001), and the carbonate rocks formed during this period are major targets for deeply buried oil and gas exploration worldwide, including China (Craig et al., 2009; 2010; 2013; Bhat et al., 2012; Zhao et al., 2014; Frolov et al., 2015; Zhu et al., 2015; Li et al., 2018). As a moderately clean low-carbon energy source relative to fossil fuels with high CO_2 emissions per power unit (e.g., coal) (Barbosa et al., 2020), natural gas exploration has made significant discoveries in the Precambrian carbonate strata of the Ediacaran Dengying Formation, Sichuan Basin. It includes the oldest, mono-block, and largest single reserve carbonate gas field in China (the Anyue gas field, with the Gaoshiti–Moxi (GM) area as the core body)

* Corresponding author at: State Key Laboratory of Petroleum Resources and Prospecting, China University of Petroleum, Beijing 102249, China.
E-mail address: lgd@cup.edu.cn (G. Liu).

https://doi.org/10.1016/j.jseaes.2023.105780
Received 29 October 2022; Received in revised form 25 June 2023; Accepted 25 June 2023
Available online 26 June 2023

(Zhu et al., 2015; Yang et al., 2018b). Since 2020, several exploratory wells have revealed high-yield natural gas in the Ediacaran Dengying Formation on the North–Slope (NS) of the GM area (Xu et al., 2021; Wei et al., 2022; Yang et al., 2022).

Fluids (e.g., surface water, formation water, oil, and gas) continuously fill and modify the carbonate strata after formation, during which time the reservoir quality could be improved or densified into the extinction line (Zhang et al., 2015). The mineral sequence and origin of dolomite of deeply buried carbonates are crucial because the evolution is more complex and the vertical stress is greater than in shallow formations, directly determining the ability of the reservoir to carry and store hydrocarbons (Jia and Pang, 2015). Throughout the burial evolution, the primary origin of dolomite includes syngenetic microbial (Vasconcelos and McKenzie, 1997; Baldermann et al., 2015; Guido et al., 2018), penecontemporaneous (Friedman and Sanders, 1967; Hsü and Schneider, 1973; Feng and Jin, 1994), seepage-reflux (Xiang et al., 2020; Zhou et al., 2020), and buried dolomitizations (Mattes and Mountjoy, 1980; Zenger, 1983; Wierzbicki et al., 2006). The fluid properties, temperatures, pressure conditions, and depositional environments vary from one geological setting to another. Therefore, the petrological characteristics (Fairchild and Spiro, 1987; Bahnan et al., 2021), isotopes (C–O–Sr isotope) (Fairchild and Spiro, 1987; Zempolich et al., 1988; Burns et al., 1994; Feng et al., 2017; Su et al., 2022), trace and rare earth element (REE) distribution patterns and related element contents (e.g., Mn, Sr, Fe, Ba, Cu, and Mg) of the reservoir rocks can be used to trace their origins (Warren, 2000; Nothdurft et al., 2004; Zhou et al., 2020; Shembilu et al., 2021). With the improvement in in-situ ablation technology, single mineral targets can be accurately analyzed to avoid intermineral interference and sample extraction difficulties (Bruguier et al., 2020), and micro, macro, geochemical, and geological evidence can intervalidate through basin modeling (Bahnan et al., 2021). Scholars have researched the Ediacaran Dengying Formation in the central Sichuan Basin. For example, Zhou et al. (2020) proposed three models based on isotope and elemental geochemistry: syngenetic microbial, penecontemporaneous reflux, and burial dolomitizations. Jiang et al. (2016) and Feng et al. (2017) verified the contribution of hydrothermal fluids to dolomite formation, and Jin et al. (2019) proposed a microbial-involved seawater seepage-reflux model. Chen et al. (2017) found microscopic spherical dolomite in their study, which is direct evidence of microbial involvement (Vasconcelos and McKenzie, 1997; You et al., 2014). Zhao et al. (2021) revealed the significance of the aragonite–dolomite sea represented by fibrous dolomite. The above studies show the complexity of the Precambrian marine carbonate strata, i.e., the fluid and origin of dolomite in reservoirs is diverse over an extended geologic time (~542 Ma; Shergold and Cooper, 2004), and there might be multiple dolomitization mechanisms. Isotopic and elemental data that carry and record fluid information are also subject to fractional alterations, requiring multiple methods for identification and characterization combined with geologic evolutionary processes. As an inherited large uplift, the GM and NS areas provides an ideal site for systematically investigating this subject.

In this study, based on the latest drilling cores, we started from the reservoir mineral sequence investigation and combined it with the qualitative analysis of petrology, fluid inclusions, C–O–Sr isotope, ordering degree, trace elements, and REE (including in-situ tests). This research aims to clarify the petrological sequence of the Ediacaran Dengying Formation in the NS and GM areas and the fluid properties and origin of each dolomite phase to establish a unified evolutionary model.

2. Geological setting

The Sichuan Basin is a large, superimposed basin in southwest China, covering approximately 18×10^4 km^2. The basin is divided into six tectonic units: Western, Northern, Central, Eastern, Southern, and Southwestern Sichuan, of which the central Sichuan Basin is in the center. The basin has undergone a vertical sedimentary transition, specifically marine deposits from the Late Ediacaran to Middle Triassic, followed by continental foreland deposits. The Ediacaran Dengying Formation in the GM area is currently a dome-shaped anticline with a burial depth of 4700–5500 m (Fig. 1A). However, no large structural traps occur in the NS area, but a series of lithological traps. From the Indosinian to the Yanshanian, the monoclinic structures in the NS area gradually evolved and finalized, and currently, the difference in burial depth of the Ediacaran Dengying Formation in the GM area can exceed 3000 m.

The Ediacaran Dengying Formation is divided into the DY1, DY2, DY3, and DY4 Members, where the gas reservoirs are distributed in the DY2 and DY4. The lithology of the reservoir is dolomite, primarily comprising multisuperimposed algal mounds and granule-shoal buildups, and the overall thickness of the formation can reach up to 800 m (Fig. 1B). The Tongwan-I and -II movements formed unconformity, leading to weathering karstification, effectively improving the pore space of the Ediacaran Dengying Formation (Wang et al., 2014b). Owing to the rifting effect within the basin, the Ediacaran Dengying Formation pinched out toward the Deyang–Anyue rift trough in the west (Wei et al., 2022). The shales of the Cambrian Qiongzhusi Formation are of the best quality, the thickest in the rift trough, and thinner in the carbonate platform due to the filling leveling-up (Song, 1996). Furthermore, the source rocks include the Ediacaran Doushantuo Formation and the DY3, dominated by mudstone, black shale, and argillaceous dolomite. Multiple uplifts, denudation, and subsidence occurred in the central Sichuan Basin (Fig. 1C). The Ediacaran Dengying Formation was buried at 2500–3000 m in the Late Caledonian, and high-intensity uplift occurred in the Hercynian, followed by a deep burial from the Indosinian to Yanshanian. Finally, the strata were uplifted in the Himalayan after a maximum burial depth of 7000–9000 m to form the present-day tectonic features.

3. Materials and methods

3.1. Materials

We observed and sampled the Ediacaran Dengying Formation cores from 11 drilled wells in the GM and NS areas, and more than 100 samples were obtained. Transmitted light, cathodoluminescence (CL), and scanning electron microscopy (SEM) observations were performed on 10 samples. Two thin sections were selected for the fluid inclusion test and four for in-situ elemental analysis using laser-ablation (LA) inductively coupled plasma (ICP) mass spectrometry (MS). Finally, we extracted powder samples (200 mesh) using a microdrill and agate mortar, based on the grain size, morphological characteristics, color, and contact relationship on the hand specimens. Seventy-two samples were evaluated for C–O isotope, 22 for trace elements and REE, and 20 for Sr isotope and x-ray diffraction (XRD). Table S shows the test results.

3.2. Methods

After observing the hand specimens, double-polished thin sections were made, including cast and CL thin sections, with approximately 0.05 and 0.03 mm thicknesses, respectively. Cast thin sections were impregnated with blue epoxy resin under vacuum conditions to highlight the location and morphology of the pore space. The transmitted light observation was performed on a Leica DM4500P microscope, and the CL analysis was conducted using a CL8200-MK5 CL instrument. The sample chamber was evacuated, and the electron beam generated by the CL instrument interacted with minerals at accelerating voltages of 8–25 kV. The homogenization temperature (Th), melting ice temperature, and salinity analysis of fluid inclusions were performed on a Leica DM2500P microscope and a LINKAM THMS600 cooling-heating stage (Bodnar, 1993). The Sr isotope was evaluated as follows: powder samples were dissolved with hydrofluoric and perchloric acids to form chlorides, and the strontium was separated by conventional cation exchange using an

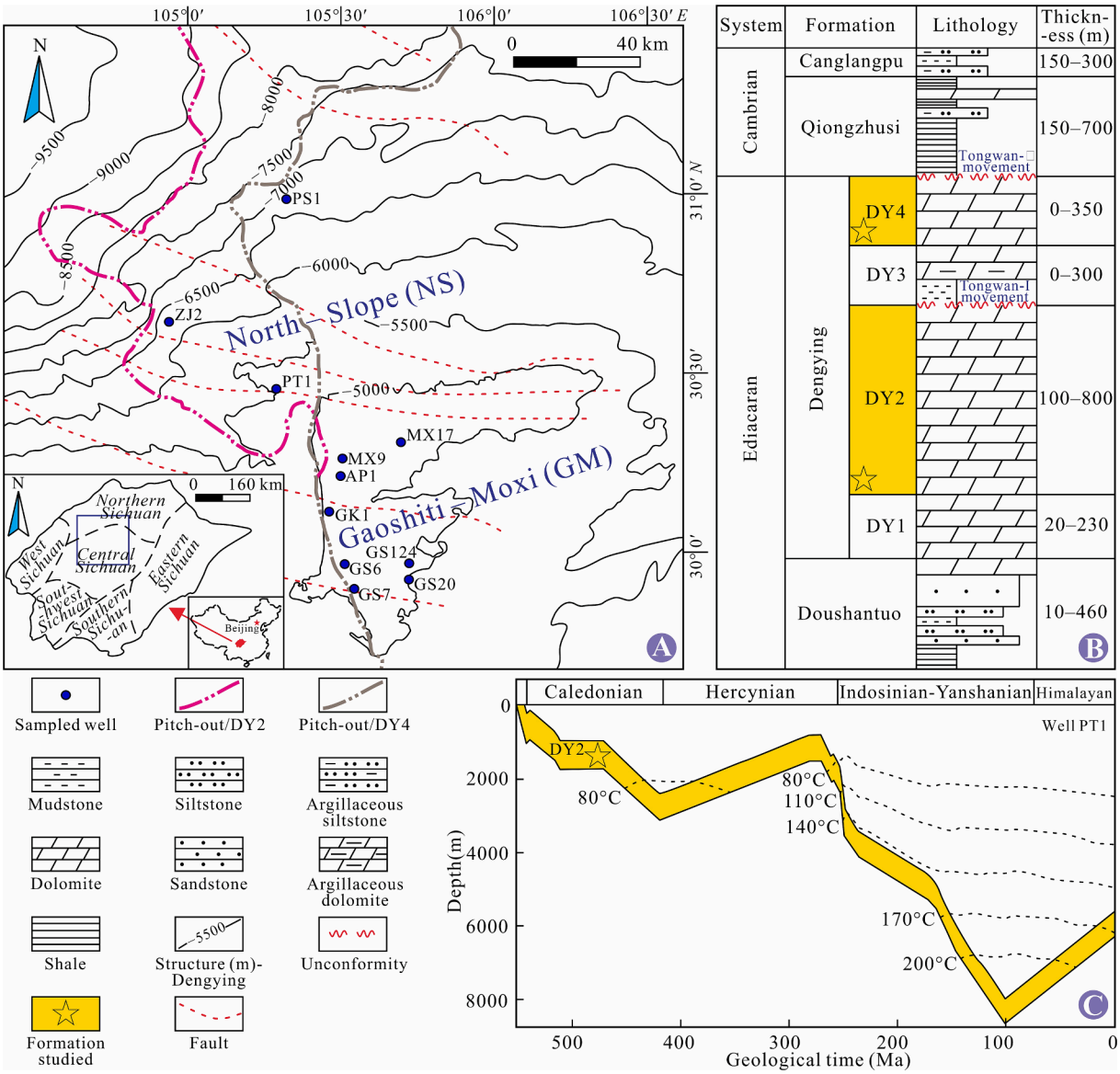

Fig. 1. Geological structure (A), stratigraphic overview (B), and burial history (C) of the Ediacaran Dengying Formation in the Gaoshiti–Moxi (GM) and North–Slope (NS) areas, central Sichuan Basin (modified after Zhu et al., 2015; Xu et al., 2021; Li et al., 2022; Yang et al., 2022).

ion exchange resin and analyzed using a Phoenix thermal ionization mass spectrometer. The test results were normalized using the internal standard of $^{88}Sr/^{86}Sr = 8.37521$, and the stability during the data acquisition was evaluated using the international standard NBS-987. Powder samples of approximately 40 mg were quantitatively selected and fully dissolved with hydrofluoric and nitric acids in a closed polytetrafluoroethylene bomb at 185 °C. Then, the hydrofluoric acid was evaporated, the solution was dissolved again, diluted to a constant volume, and measured using ICP-MS (ELEMENT XR). The above analysis was conducted at the Analytical Laboratory of the Beijing Research Institute of Uranium Geology.

The 100% phosphoric acid and the sample powder reacted at 75 °C for 12 h, and the generated CO_2 was evaluated using an Elementar Isoflow-precision isotope ratio mass spectrometer under carrier gas (99.99% helium). The standard samples used were GBW04405 ($\delta^{13}C_{VPDB}$: 0.57‰, $\delta^{18}O_{VPDB}$: −8.49‰), IAEA-CO-1-Marble ($\delta^{13}C_{VPDB}$: 2.492‰, $\delta^{18}O_{VPDB}$: −2.37‰), and IAEA-CO-8-Calcite ($\delta^{13}C_{VPDB}$: −5.764‰, $\delta^{18}O_{VPDB}$: −22.7‰). The C–O isotope test results are provided in Vienna Pee Dee Belemnite (VPDB) standardization with analytical precision higher than ±0.2‰ and ±0.3‰. The above analysis was conducted at the State Key Laboratory of Petroleum Resources and Prospecting at the China University of Petroleum, Beijing (CUPB). Fresh sections were selected, and the surface was sprayed with Au. Then, SEM observations were performed on an FEI Quanta 200F coupled with an energy dispersive spectrometer (EDS) to quantify the elemental content of the targets. The device has a maximum magnification of 25–200 K and a resolution of 1.2 nm at accelerating voltages of 0.2–30 kV. This analysis was conducted at the Microstructure Laboratory for Energy Materials, CUPB. The powder samples were flat and uniformly pressed in a carrier slot and analyzed on a Bruker D8 ADVANCE X-ray diffractometer with a wide angle of 5°–90° CuKα radiation. The tube voltage and current were 40 kV and 30 mA, respectively. The ordering degree of the dolomite is defined as the diffraction peak intensity ratios corresponding to the crystal plane (0 1 5) and (1 1 0) dolomite (typically with 2θ of 35.3° and 37.3°, respectively) (Goldsmith and Graf, 1958). This analysis was conducted at the State Key Laboratory of Heavy Oil Processing, CUPB.

The LA-ICP-MS elements were evaluated as follows: sample sections were placed in the GeolasPro LA system, the generated aerosol was transferred in a closed tube by helium gas, and the elemental content

was analyzed using an Agilent 7900 ICP-MS. The laser spot diameter was 44 μm, and the external standards were BHVO-2G, BCR-2G, and BIR-1G. The above analysis was conducted at the Wuhan Sample Solution Analytical Technology Co. Ltd., Wuhan, China. The detailed experimental procedure is described by Liu et al. (2008).

4. Results

4.1. Petrology characteristics

4.1.1. Dolomite

The content and distribution of the host rock in the Ediacaran Dengying Formation in the Sichuan Basin are dominant, showing gray and dark gray. The host rock is primarily micrite, and some primary microbial structures (e.g., algal grain clots, algal lamellae, and fibrous texture) are usually visible (Figs. 2 and 3), as well as bacteria-shaped spheroidal dolomite (Fig. 4). Typically, the host rock is dense and has a carbonate texture farthest from the residual pores filled with late dolomite (dolomite-2) and bitumen (bitumen-2), and the remaining space is the present-day natural gas storage site. The host rock appears dark and black under the microscope because of the weak light transmission. The Ediacaran Dengying Formation host rock in the Sichuan Basin is nonluminous or weakly luminous, showing dark red or black under CL (Fig. 3), the primary component of reservoir rocks.

Dolomite-1 can be observed in the hand specimens and thin sections adjacent to the host rock. Its crystal size is greater than that of the host

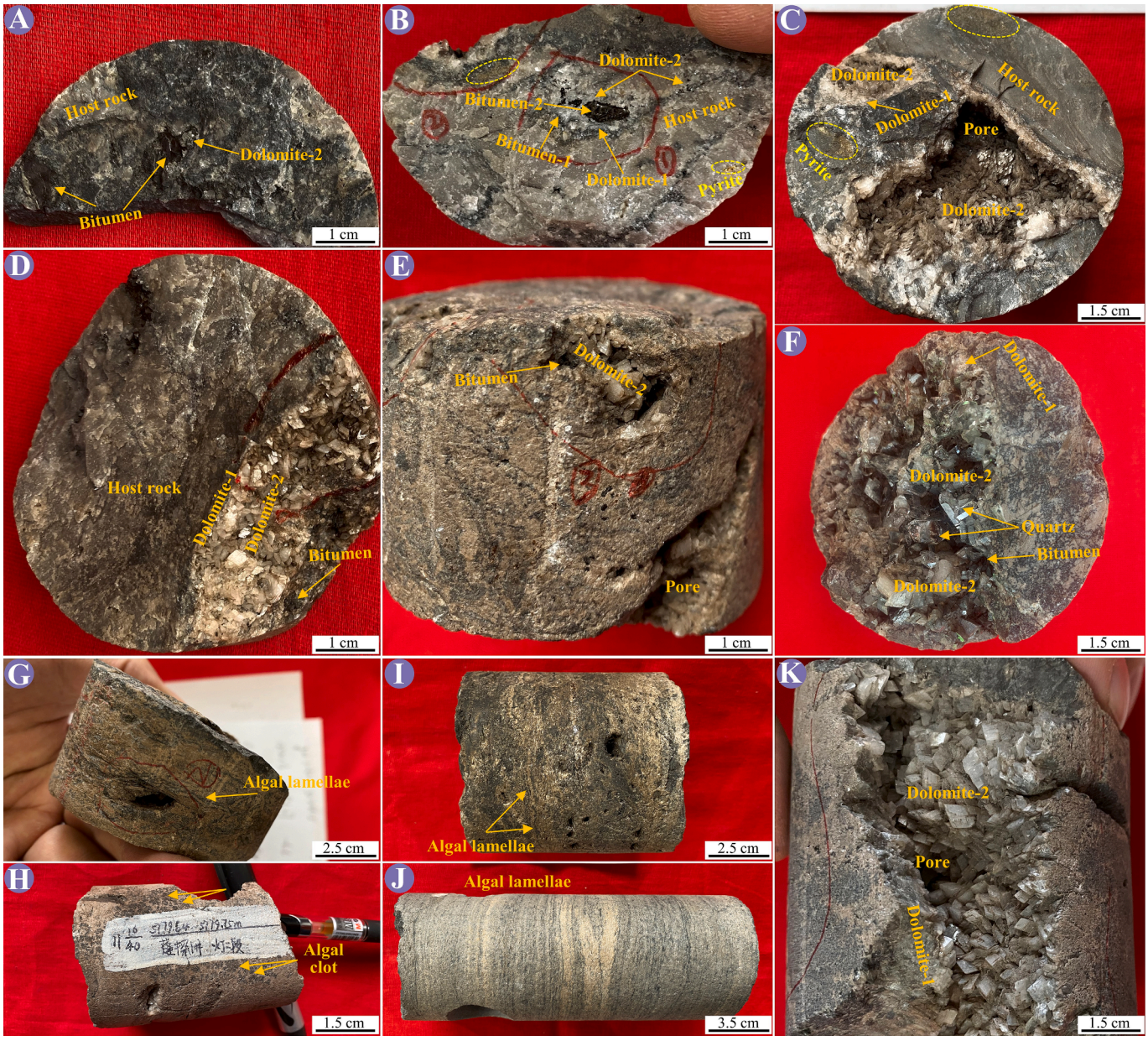

Fig. 2. Typical core characteristics of the Ediacaran Dengying Formation in the GM and NS areas, central Sichuan Basin. (A) Dolomite-2 contacts bitumen (PS1, 7260.36 m, DY4). (B) Sequentially developed dolomite-1, bitumen-1 (in thin annular bands), dolomite-2, and bitumen-2 (massive), with pyrite (PS1, 7263.55 m, DY4). (C) Dolomite-2 is present in large caves (PT1, 5768.84 m, DY2). (D) Fine crystalline dolomite-1, euhedral dolomite-2, and massive bitumen (PT1, 5791.45 m, DY2). (E) The pores are filled with dolomite-2 of large particle size, in close contact with massive bitumen-2 (PT1, 5778.20 m, DY2). (F) Away from the host rock, dolomite-1 and dolomite-2 (with medium-coarse crystals) in the pores (rhombic, saddle-shaped), and prismatic quartz (GS20, 5209.39 m, DY4). (G–J) Algal lamellae and algal clots associated host rock (GS6, 5361.8 m, DY2; PT1. 5779.64, DY2; PS1, 7260.28 m and 7266.38 m, DY4). (K) Euhedral dolomite-2 (GS20, 5194.33 m, DY4).

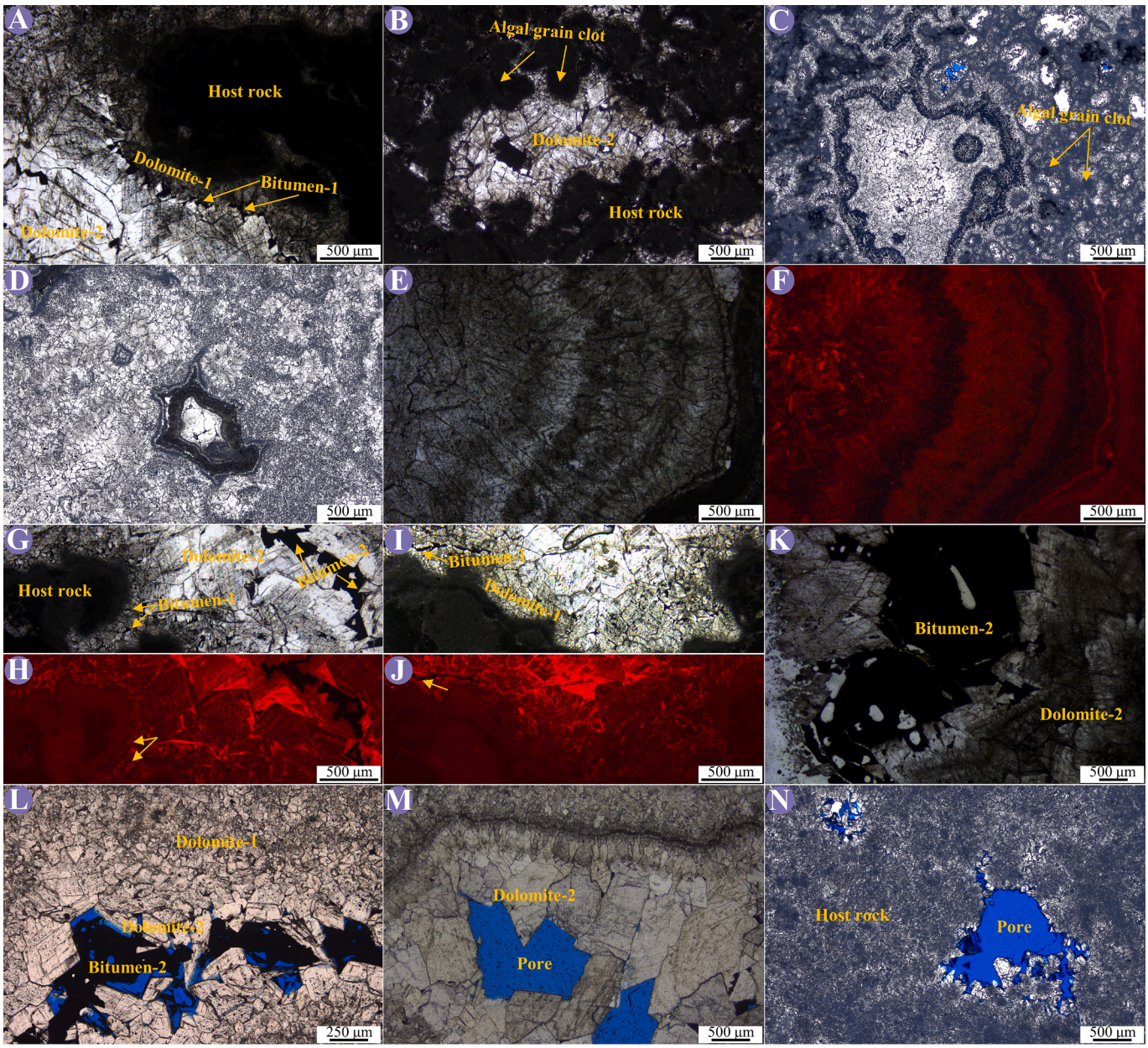

Fig. 3. Microscopic characteristics of thin sections of the Ediacaran Dengying Formation in the GM and NS areas, central Sichuan Basin. (Note: PPL, plane-polarized light; CL, cathodoluminescence). (A) PPL, the black host rock is bordered by dolomite-1, early annular bitumen-1, and bright dolomite-2 (PS1, 7267.80 m, DY4). (B) PPL, host rock associated with algal grain clots (GS20, 5209.56 m, DY4). (C–D) PPL, algal grain clots and microbial related host rock (PT1, 5773.78 m, DY2). (E–F) PPL and CL, fibrous and radial dolomite (PT1, 5733.89 m, DY2). (G–J) PPL and CL, dolomite-2 cathode luminous red bright, bright and dark luminous ring band; bitumen-1 shows black, small intrusion spots and thin layers (PS1, 7270.17 m, DY4). (K) PPL, dolomite-2 is rhombic and saddle-shaped, and massive bitumen-2 (GS20, 5183.47 m, DY4). (L) PPL, the blue area is the residual harbor-like shape pore cast (ZJ2, 6554.3 m, DY2). (M) PPL, pores filled with large amounts of dolomite-2 (PT1, 5777.24 m, DY2). (N) PPL, pores not filled with large amounts of dolomite-2 (MX39, 5307.16 m, DY4). (For interpretation of the references to color in this figure legend, the reader is referred to the web version of this article.)

rock but also small, belonging to the fine–medium crystal dominated by anhedral dolomite. The color of dolomite-1 is slightly brighter than that of the host rock but still has a dark and dirty luster compared with dolomite-2 in the pore center and is weakly luminescent and dominated by dark red under CL. Classifying dolomite textures is typically based on the crystal size and boundary shape (Sibley and Gregg, 1987), and dolomite-2 is well characterized and distinguished from the host rock and dolomite-1. It has coarse grains widely developed in pores away from the host rock, a few millimeters to more than 1 cm (Fig. 2F, K). The hand specimen of dolomite-2 is white, with a clean and bright surface, accompanied by some mist-centered bright-edged structures. Furthermore, the crystals are highly euhedral, typically rhombic, with some nonplanar saddle- and sickle-shaped crystals (Figs. 2, 3, and 4). Mineral crystals typically grow toward the pore center and show wave extinction under crossed-polarized light (Fig. 5). The color is bright, from dark red to bright red under CL, which is related to its high Mn contents and Mn/Fe ratio. Further, the particle edges have circular light–dark transitions and are closely adjacent to nonluminous bitumen-2. Fluid inclusions exist in dolomite-1 and dolomite-2, primarily aqueous and gas inclusions. Inclusions are more common in dolomite-2, with Th values from 115 °C to 140 °C and 130 °C to 215 °C, and the mean salinity is 22.04 w% NaCl and 17.37 w% NaCl in dolomite-1 and dolomite-2, respectively (Fig. 6).

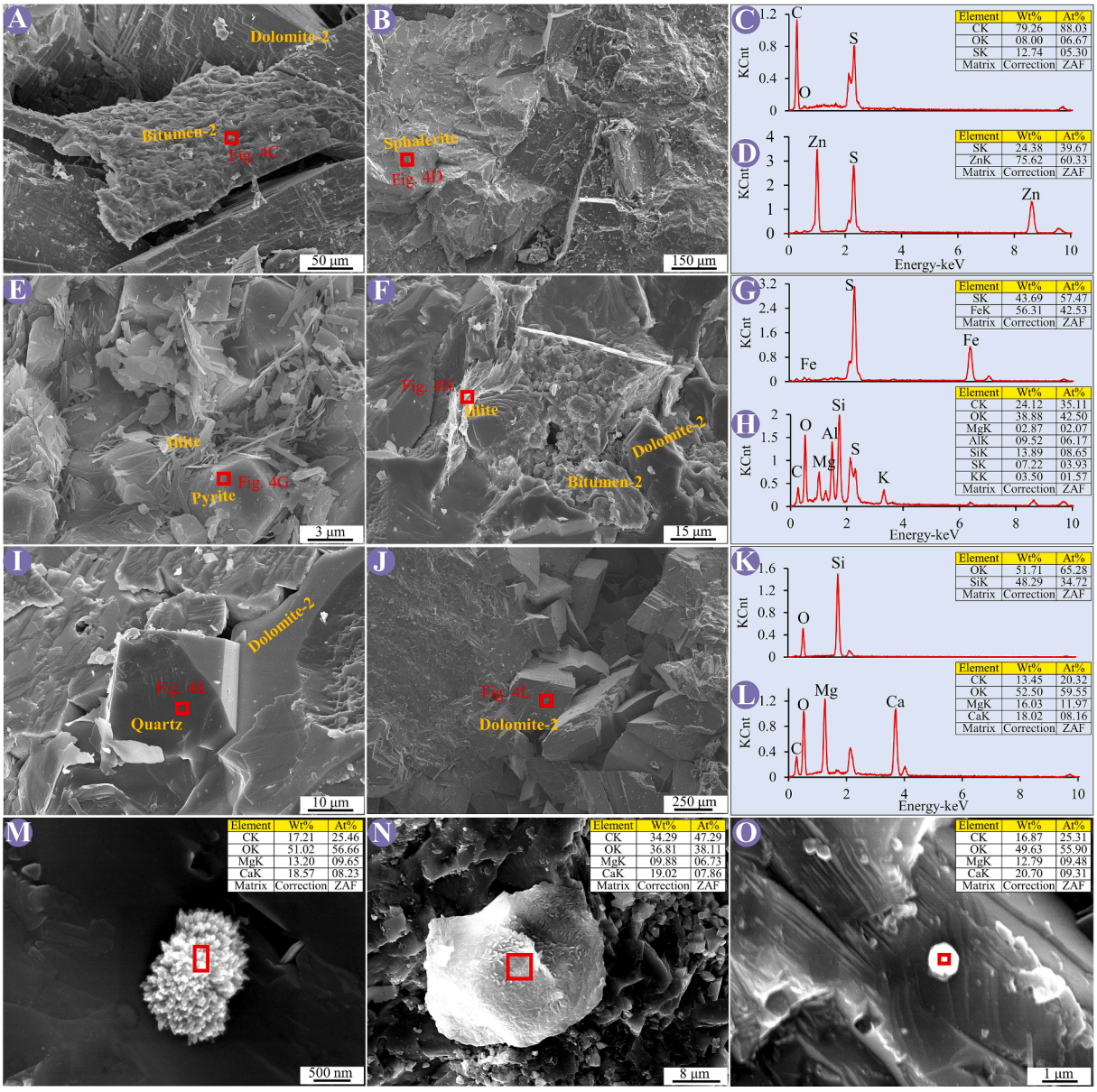

Fig. 4. Scanning electron microscopy (SEM) and energy dispersive spectrometer (EDS) characteristics of the Ediacaran Dengying Formation in the GM and NS areas, central Sichuan Basin. (A) Massive bitumen-2 distributed between particles of dolomite-2 (PS1, 7263.99 m, DY4). (B) Sphalerite on the surface of dolomite (PS1, 7263.55 m, DY4). (C) EDS data of bitumen in Fig. 4A. (D) EDS data of sphalerite in Fig. 4B. (E) Pyrite is associated with illite (PT1, 5775.2 m, DY2). (F) Illite and bitumen-2 are present between dolomite-2 grains, while fully prismatic regular euhedral quartz develops (I) (GS7, 5293.44 m, DY4). (G) EDS data of pyrite in Fig. 4E. (H) EDS data of illite in Fig. 4F. (J) Euhedral dolomite-2 with large grain size, rhombic and saddle-shaped (GS6, 5365.00 m, DY2). (K) EDS data of quartz in Fig. 4I. (L) EDS data of dolomite in Fig. 4J. (M–O) Bacteria-shaped dolomite in the host rock (PT1, 5785.37 m, DY2; GS7, 5264.52 m, DY4).

4.1.2. *Bitumen*

Bitumen-1 is uncommon in core and thin sections because of its small size and limited distribution. It is typically distributed between dolomite-1 and dolomite-2 as black, thin layers, films, or small intrusion spots and does not emit light under CL (Fig. 2B and 3A, G–J). Bitumen-2 is typically massive, large, and widely distributed in the Ediacaran Dengying Formation, with some fully filled and some partially filled pore spaces. Bitumen-2 adheres to dolomite-2 without changing its crystal boundary texture, indicating that bitumen-2 formed later than dolomite-2. Bitumen-2 is black and opaque and has various shapes under the microscope (e.g., rod-like, polygonal), conforming to the geometry of the pore space (Figs. 2, 3, 4, and 5). Under SEM, the bitumen-2 is massive, crust-like, and sheet-like, and the EDS data show that the bitumen primarily comprises C, O, and S (C dominance). Bitumen-2 has a grayish-metallic luster under reflected light and might have different coke structures, depending on its maturity or precursors (Gao et al., 2018).

4.1.3. *Quartz and metallic minerals*

Quartz is present in pores only partially filled with large amounts of massive bitumen-2. Quartz is a euhedral granular with a transparent to translucent glass luster, except for a few anhedral textures. Giant quartz over 1.5 cm in length can be observed in the core and is clean and transparent in the thin section. In some samples, quartz directly contacts dolomite-2 due to the absence of bitumen-2 (Figs. 4 and 5P–R). However, in others, the complete sequence of dolomite-2, bitumen-2, and quartz is well-preserved (Fig. 2F). Furthermore, there are negligible amounts of metal (e.g., pyrite, and sphalerite) and clay (e.g., illite) minerals (Fig. 4).

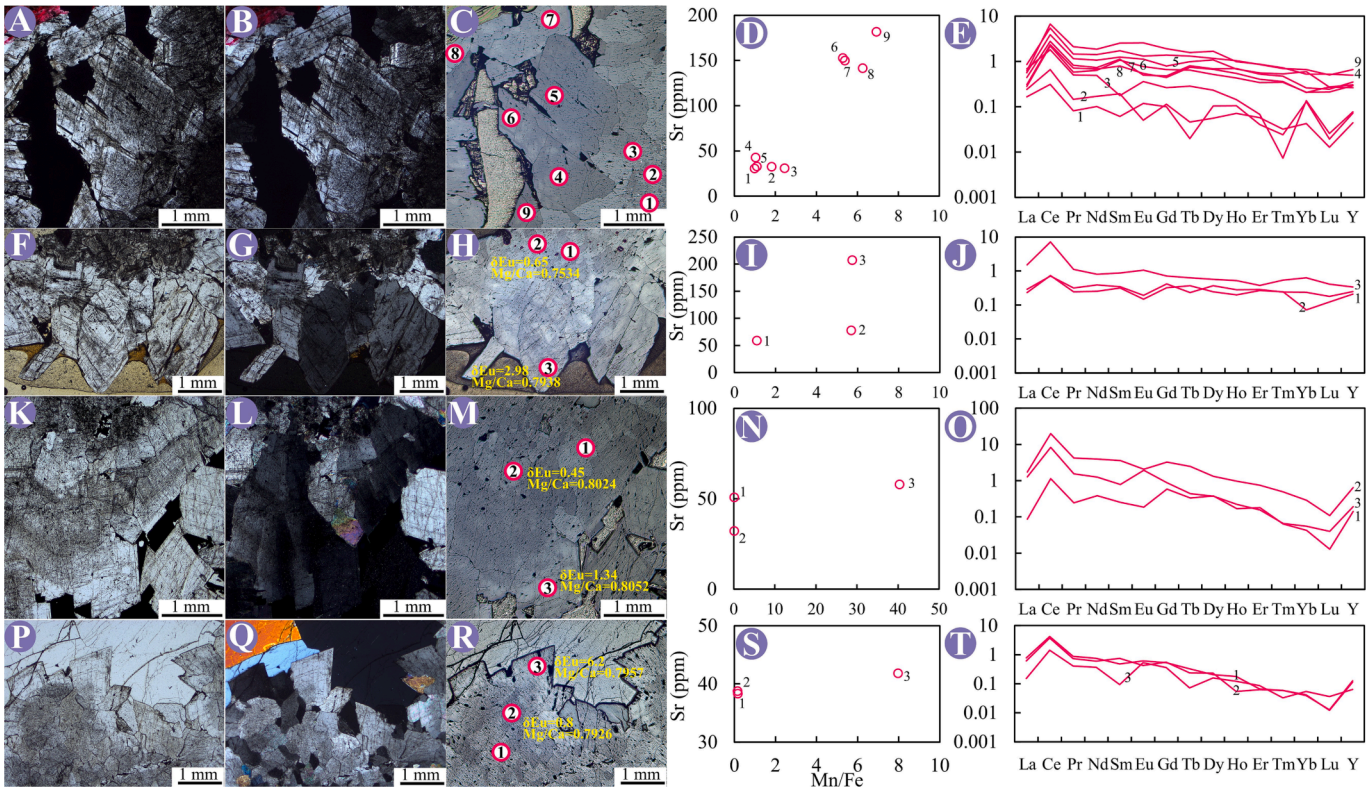

Fig. 5. LA-ICP-MS elements and distribution of the relevant parameters (Mn/Fe versus Sr content, seawater ($\times 10^6$)-normalized REE patterns) of the Ediacaran Dengying Formation in the GM and NS areas, central Sichuan Basin. In-situ test targets were identified after plane-polarized, crossed-polarized, and reflected light. Dolomite-2 shows wave extinction under crossed-polarized light, and bitumen shows a fine-grained mosaic under reflected light. (A–E) PS1, 7263.55 m, DY4. (F–J) PT1, 5789.85 m, DY2. (K–O) GS20, 5183.47 m, DY4. (P–T) GS124, 5566.9 m, DY4. Data on the average Pacific seawater were sourced from Kawabe et al. (1998) and Tepe and Bau (2016).

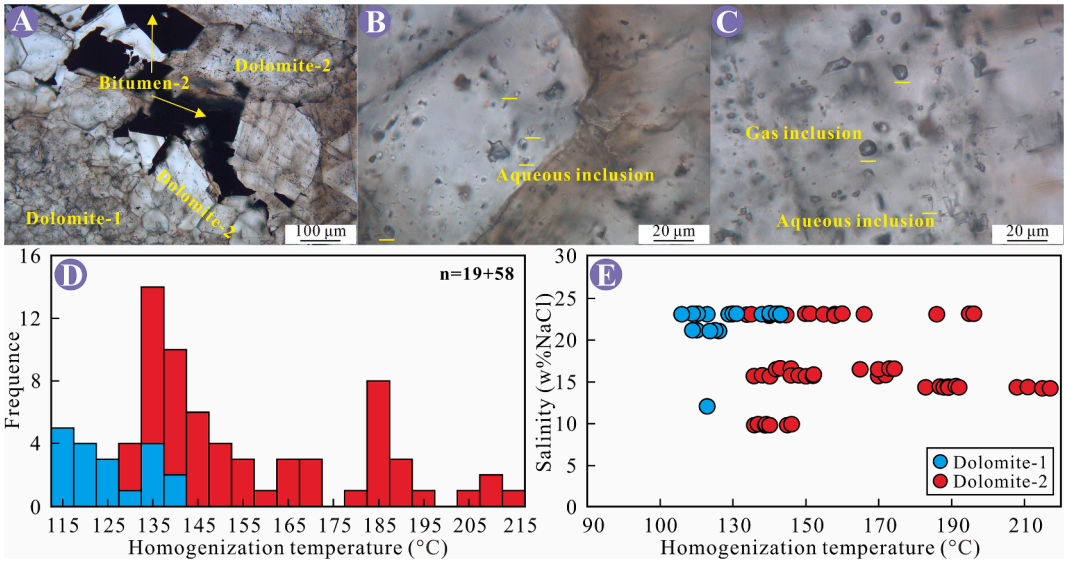

Fig. 6. Microscopic characteristics, homogenization temperature, and salinity distribution of fluid inclusions in dolomite-1 and dolomite-2 of the Ediacaran Dengying Formation.

4.2. C–O–Sr isotope characteristics

The $\delta^{13}C_{VPDB}$ and $\delta^{18}O_{VPDB}$ values of the host rock were 0.65‰ to 2.64‰ (avg. 1.78‰) and −10.73‰ to −1.88‰ (avg. −6.99‰), and those of dolomite-1 were −0.98‰ to 1.71‰ (avg. 0.75‰) and −12.63‰ to −6.85‰ (avg. − 9.96‰), with $^{87}Sr/^{86}Sr$ values of 0.708701–0.709273 (avg. 0.708874) and 0.709213–0.709952 (avg. 0.709583), respectively. The $\delta^{13}C_{VPDB}$ and $\delta^{18}O_{VPDB}$ values of dolomite-2 were lower than the host rock and dolomite-1, whereas the $^{87}Sr/^{86}Sr$ values were greater, from −3.00‰ to 1.43‰ (avg. −0.47‰), −13.56‰ to −9.93‰ (avg. −11.03‰), and 0.709930 to 0.712022 (avg. 0.711274), respectively (Table S; Fig. 7).

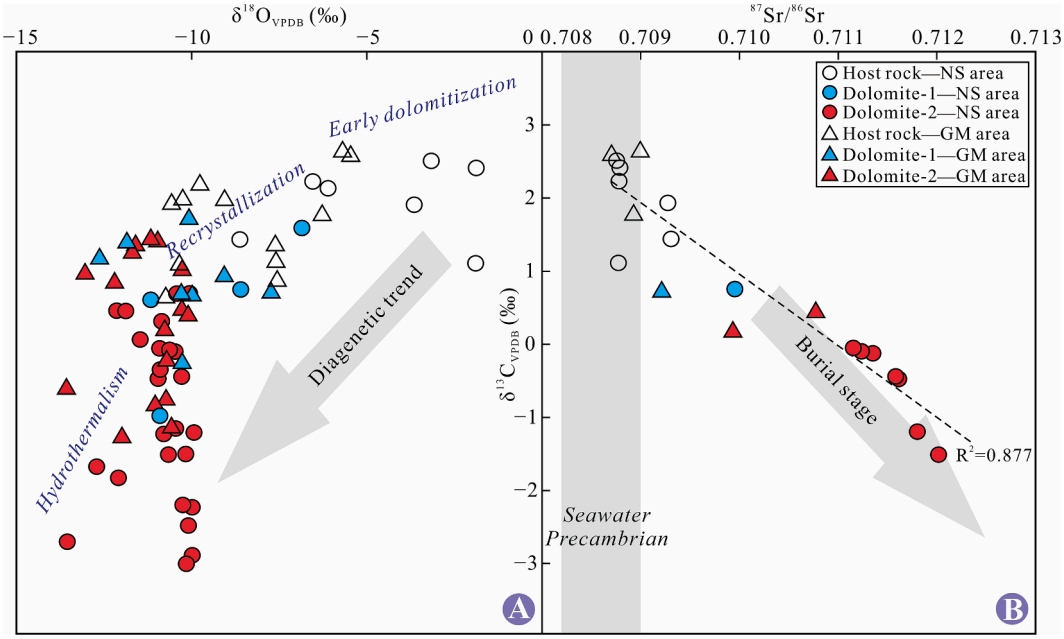

Fig. 7. $\delta^{13}C_{VPDB}$, $\delta^{18}O_{VPDB}$, and $^{87}Sr/^{86}Sr$ values of the Ediacaran Dengying Formation in the GM and NS areas, central Sichuan Basin. $^{87}Sr/^{86}Sr$ values of coeval seawater were from Burns et al. (1994).

4.3. Ordering degree characteristics

Fig. 8 shows the calculation of the ordering degree, with the lowest value (avg. 0.75) for the host rock. The average ordering degree of dolomite-1 and dolomite-2 was 0.76 and 0.87 (0.70–1.00), respectively, showing a high ordering degree and sufficient growth space during the dolomite-2 formation period. However, the ordering degree of some host rock samples was high, reaching 0.95.

4.4. Major and trace elements

The Mg and Ca contents in various dolomites were high, accounting for 95% to 99% of the sum of dolomite-1 and dolomite-2. The Mn/Fe ratio of dolomite-1 was 0.15–5.69 (avg. 1.41), whereas that of dolomite-2 was 1.03–40.38 (avg. 8.90). The Sr content in dolomite-1 was 37.7–73.3 ppm (avg. 57.07 ppm), and in dolomite-2 was 42–147 ppm (avg. 111.44 ppm). The host rock has the lowest Sr content, from 29.6 to 57.4 ppm (avg. 43.63 ppm). The Sc, Th, Hf, and Zr contents were very low, with average values of 0.422, 0.142, 0.068, and 0.425 ppm in the host rock, 0.321, 0.025, 0.020, and 0.801 ppm in dolomite-1, and 0.517, 0.019, 0.023, and 0.303 ppm in dolomite-2, respectively. Furthermore, the Rb/Sr ratios were 0.0262 (0.0027——0.1843), 0.0047 (0.0009——0.0091), and 0.0009 (0.0005——0.0016), respectively.

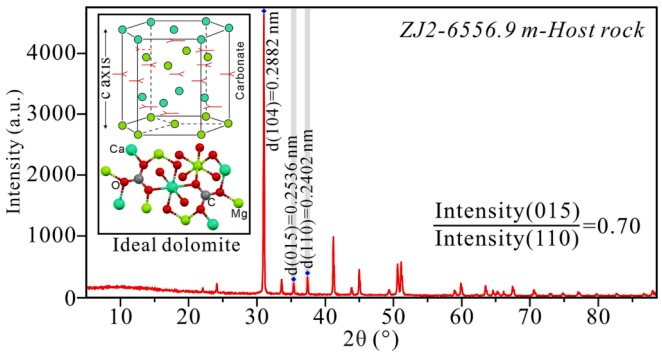

Fig. 8. Schematic calculation of the dolomite ordering degree based on X-ray diffraction (XRD). The ideal dolomite structure model was modified after Land, 1985 and Warren, 2000.

4.5. Rare earth elements (REE)

Table S summarized the REE results. The total REE (∑REE) contents in the host rock, dolomite-1, and dolomite-2 were 1.872——12.488 ppm (avg. 5.784 ppm), 7.964——12.327 ppm (avg. 10.040 ppm), and 20.933——32.115 ppm (avg. 25.010 ppm), respectively. The total light REE (LREE) and heavy REE (HREE) showed the same rule; the mean ∑LREE values were 3.077 ppm, 4.768 ppm, and 13.734 ppm, and the ∑HREE values were 0.641 ppm, 1.402 ppm, and 3.106 ppm, respectively. Furthermore, the REE distribution patterns of all dolomites show enrichment in LREE and depletion of HREE, with ∑LREE/∑HREE ratios of 5.449, 3.448, and 4.492. The Y/Ho ratios of the host rock, dolomite-1, and dolomite-2 were 48.9, 44.1, and 43.3, respectively.

5. Discussion

5.1. Sample reliability evaluation

Although the samples are finely selected, it is challenging to avoid contamination (e.g., sample preparation). Terrestrial particulate matter, Fe and Mn oxides, and phosphates primarily affect the REE of marine carbonate (Nothdurft et al., 2004). Therefore, data reliability evaluation is necessary for elemental analysis, and the elemental characteristics of the samples with less contamination are more dependable. The ΣREE of terrigenous particulate matter was typically greater than 100 ppm (e.g., Post-Archean Australian Shale (PAAS)–211.37 ppm, Upper Continental Crust (UCC)–168.37 ppm, and Ocean Island Basalt (OIB)–227.96 ppm; Taylor and McLennan, 1985; Sun and McDonough, 1989; McLennan, 2001). However, all our dolomite samples were 1.872–32.115 ppm (avg. 15.103 ppm), indicating that the contamination caused by terrigenous detritus is negligible because if there are few mixed inputs, the impact on the sample test values will also be significant (Nothdurft et al., 2004). The Sc, Th, Hf, and Zr contents of the samples are much lower than the reported values of PAAS (16, 14.6, 5, and 210 ppm) and UCC (13.6, 10.7, 5.8, and 190 ppm), and no dependable positive correlation occurs between ΣREE and Fe and P contents (Fig. 9A–B). Therefore, the influence of Fe and Mn oxides and phosphates on incorporating REE in the

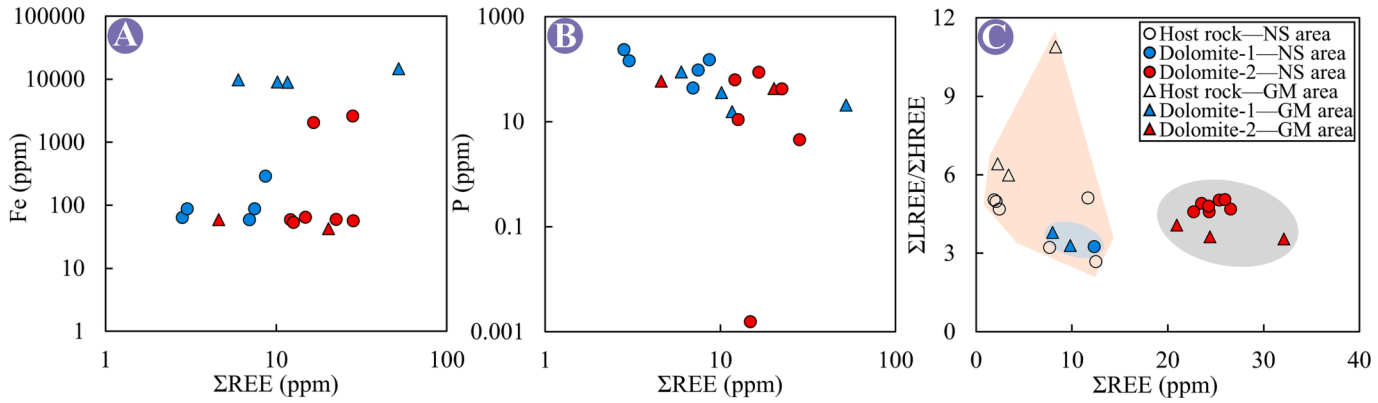

Fig. 9. Correlation diagram between ΣREE and Fe (A), P content (B), and ΣLREE/ΣHREE (C) of the Ediacaran Dengying Formation in the GM and NS areas, central Sichuan Basin.

samples is minimal. Furthermore, the Y/Ho ratio in terrigenous sediments was 26–28, whereas that of seawater and marine sediments was 44–73 (the average value in nonclastic marine sediments is 45.5) (Bau and Dulski, 1996; Webb and Kamber, 2000; Tepe and Bau, 2016), and 34.15–62.42 in our samples (avg. 45.70) (Fig. 10), indicating low contamination.

The C–O–Sr isotope of the three dolomite samples show a specific correlation, especially between $^{87}Sr/^{86}Sr$ and $\delta^{13}C_{VPDB}$ ($R^2 = 0.877$), reflecting the validity of the isotope data. However, information in the ordering degree of dolomite must be treated with caution. The ordering degree of dolomite indicates the crystallization degree, reflecting the physical and chemical conditions of its formation period. Compared to the arrangement of Ca and Mg molecular layers in ideal dolomite, natural dolomite shows super-structured reflections because of multiple factors (e.g., medium composition, temperature, pressure, crystallization rate, and geological evolution) (Manche and Kaczmarek, 2021). In the burial process, dolomite will gradually develop into ordered cells with a gradual increase in the ordering degree. Typically, the average ordering degrees of the sample were 0.75, 0.76, and 0.85 in the host rock, dolomite-1, and dolomite-2. However, some samples, such as the host rock from well PS1 in the NS area (7263.55 m), have a value of 0.95 because during deep burial evolution, when the increase in the ordering degree reaches a specific critical point, it will increase irregularly, therefore, the values of the early-stage dolomite might also be high (Zhang et al., 2014a). Further, the buried depth of the sample from well PS1 is the largest among all, and the maximum burial depth in the historical period might reach 9500 m (inferred from Fig. 1C), therefore, it is most likely to reach an irregular increase state.

5.2. Fluid properties recorded by dolomite

The $\delta^{13}C_{VPDB}$ and $\delta^{18}O_{VPDB}$ of dolomite are controlled by the isotopic composition of the dolomitized minerals, the salinity, and the temperature of the fluid and are closely related to the isotopic background values of seawater. $\delta^{13}C_{VPDB}$ records the global carbon cycle process, e.g., ocean cycle, productivity, and terrigenous clastic supply. $\delta^{13}C_{VPDB}$ is significantly affected by organic matter and thermochemical sulfate reduction and less by temperature. Moreover, the carbon concentration of carbonate rocks is remarkably higher than diagenetic fluid; therefore, producing superposition and disturbing its geological record significance is challenging. However, when the water/rock ratio is greater than 1000, recrystallization will reduce the $\delta^{13}C_{VPDB}$ value. Theoretically, $\delta^{18}O_{VPDB}$ responds to the parameters of seawater oxygen $\delta^{18}O_{VPDB}$ and temperature in geological time and is sensitive to changes in pore water, oxygen exchange, recrystallization, and the water/rock ratio under high temperatures (Fairchild and Spiro, 1987; Zempolich et al., 1988; Feng et al., 2017; Su et al., 2022). Recrystallized new cementation products reduce the $\delta^{18}O_{VPDB}$ values. Typically, low $\delta^{18}O_{VPDB}$ values show enrichment in ^{16}O and depletion of ^{18}O, indicating formation in a medium to deep burial environment at high temperatures. $\delta^{18}O_{VPDB}$ values less than −5‰ and −10‰ represent partial and strong alteration, respectively. Tectonic and deep thermal fluid activities can cause early dolomite recrystallization, and its $\delta^{18}O_{VPDB}$ values also drop rapidly, usually less than −10‰ (Kaufman and Knoll, 1995; Feng et al., 2017). Sr is a crucial constituent element in seawater, where the weathering of materials from different sources and thermal fluid modification forms the final equilibrium $^{87}Sr/^{86}Sr$ values. The residence time of Sr in the modern ocean (2.4 Myr) is more than 1000 times longer than the mixing cycle time of the ocean (1.5 Kyr) (Krabbenhöft et al., 2010); therefore,

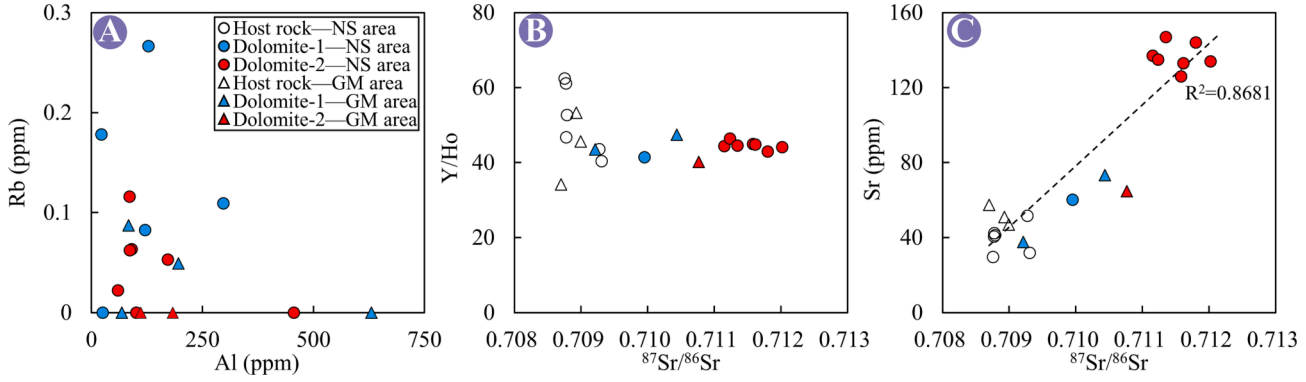

Fig. 10. Correlation diagram of Al and Rb contents(A), and $^{87}Sr/^{86}Sr$ versus Y/Ho ratio (B) and Sr content (C) of the Ediacaran Dengying Formation in the GM and NS areas, central Sichuan Basin.

the global seawater should have been well mixed and homogeneous during the historical period, which is why we can use the North American Precambrian seawater for comparison. The $^{87}Sr/^{86}Sr$ values of carbonates progressively increase after deposition because large amounts of potassium-bearing silicates (enriched in radiogenic ^{87}Rb and gradually decaying to ^{87}Sr, and thus high $^{87}Sr/^{86}Sr$; Steiger and Jäger, 1977) release ^{87}Sr into the fluids, and fluid diagenesis is incorporated into the new crystalline minerals of carbonate rocks (Fairchild et al., 2018). Most Rb in sedimentary rocks is distributed in the weathered products of igneous rocks (especially rich in continental crust but low in mantle and oceanic crust) and in potassium-rich clay minerals, and the deep thermal fluids at midocean ridges are rich in Sr. Therefore, the covariant of C–O–Sr isotope can well trace the fluid properties and diagenetic alteration intensity during dolomite formation (Otsuji et al., 2013; Bahnan et al., 2021; Ha et al., 2021; Shembilu et al., 2021).

CL is a popular carbonate rock study tool based on the principle of ion transition. The luminescence of carbonate rocks is typically activated by Mn^{2+} and quenched by Fe^{2+} (and some other elements, e.g., Sm^{3+}, Eu^{2+}, Eu^{3+}, Tb^{3+}, Dy^{3+}, Fe^{3+}, and Ni^{2+}; Machel and Burton, 1991) (Hemming et al., 1989; Scholle and Ulmer-Scholle, 2003). These two elements are rich in atmosphere, formation, and deep fluids and can distinguish whether fluids are involved or altered (Kaufman and Knoll, 1995). Typically, dull, uniform to patchy luminescence indicates the major components, whereas bright to nonluminescence and obvious zoned bands indicate the minor components. From the host rock rich in various primary textures to the medium-coarse dolomite, the color of their transmitted light becomes brighter, the grains become larger, the euhedral degree is enhanced, and the luminous color under CL is typically brighter. However, many factors affect the CL color, intensity, and zonation of carbonate. Machel and Burton (1991) proposed at least 26 factors, including the content of potential activators, sensitizers, quenching agents, concentration ratio, and crystal surface. Therefore, synergistic analysis of CL and other features (e.g., isotopes) is necessary. The host rock, dolomite-1, and dolomite-2 of the Ediacaran Dengying Formation in the central Sichuan Basin have divergent C–O–Sr isotopic distributions (Fig. 7). The mean $\delta^{13}C_{VPDB}$ and $\delta^{18}O_{VPDB}$ values of the host rock are still smaller than the North American Precambrian seawater (5‰ to 7‰, −0.5‰ to 0.9‰; Fairchild and Spiro, 1987; Zempolich et al., 1988). However, the $^{87}Sr/^{86}Sr$ values (avg. 0.708874) are similar to the seawater background (0.70708–0.70900; Burns et al. 1994). This result shows that the fluid during the host rock formation was coeval seawater, and the depletion of $\delta^{13}C_{VPDB}$ ratio might be caused by the involvement of atmospheric CO_2 in the near-surface conditions and the inorganic–organic interactions of microorganisms (Warthmann et al., 2000; Baniak et al., 2014; Huang et al., 2021; Bai et al., 2022). The formation temperature caused the homoplastically depleted $\delta^{18}O_{VPDB}$, and the late high-temperature unavoidably altered the host rock, making the $\delta^{18}O_{VPDB}$ values more negatively biased than coeval seawater (Jiang et al., 2016; Ha et al., 2021; Bai et al., 2022). After the dolomite formation, the normal burial of the Precambrian strata experienced a high temperature of more than 200 °C (ca. 100 Ma) (Fig. 1C), which provided conditions for the altering $\delta^{18}O_{VPDB}$ values.

The dirty color of dolomite-1 could result from metasomatism or the incomplete dissolution of micrite dolomite remnants (Yang et al., 2018a). The average ordering degree is 0.76, and the fine crystal presents a mosaic texture, indicating that the space is limited during its formation or the fluid Mg/Ca and water/rock ratios involved are low. Dolomite-1 has medium C–O–Sr isotope values between the host rock and dolomite-2, indicating weak mixing of fluid under coeval seawater domination, which could be basinal brine. Basinal brine has high salinity due to the restricted space that weakens the fluid exchange, also confirmed in the salinity recorded by fluid inclusions. The salinity of the inclusions in dolomite-1 is concentrated, with an average of 22.04 w% NaCl, except for one measuring point (12.11 w% NaCl). Dolomite-2 shows extremely strong fractionation properties, with extremely depleted $\delta^{13}C_{VPDB}$–$\delta^{18}O_{VPDB}$ (mean $\delta^{18}O_{VPDB}$ value of −11.03‰, <−10‰) and enriched $^{87}Sr/^{86}Sr$ (avg. 0.7112), significantly greater than coeval seawater values, which are also higher throughout the geological history reported by McArthur et al. (2001) and Halverson et al. (2007). The highly correlated covariances of C–O–Sr isotope indicate that this is caused by the same event (Fig. 7). The Rb/Sr ratio of the sample was small (0.0005–0.0016, avg. 0.0008). The in-situ tests revealed no correlation between Al and Rb contents, $^{87}Sr/^{86}Sr$, and Y/Ho, indicating that the Sr source is not an aluminosilicate weathering product and the alteration of $^{87}Sr/^{86}Sr$ is not caused by mixing terrestrial input (Fig. 10). Therefore, a mixed input of basinal brine and deep thermal fluid dominates the dolomitization fluid of dolomite-2, increasing the radiogenic Sr content. This result coincides with its petrological characteristics, where the particle sizes formed in the fluid phase (e.g., hydrothermal fluid) become coarser, and the primary textures disappear, forming standard euhedral crystals if there is enough space.

The REE patterns of different types of dolomites are similar (Figs. 5 and 11) regarding their contents, which covary with the C–O–Sr isotope, indicating that the petrological classification is dependable. The samples all show LREE enrichment and HREE depletion, and the ΣLREE/ΣHREE ratio exceeds 3 (Fig. 9C). The reservoir rocks of the Ediacaran Dengying Formation were normalized using PAAS, UCC, Chondrite, and Seawater to eliminate the atomic abundance relationship of different odd and even numbers and find a suitable normalization model (Fig. 11A–D). The REE pattern in the sample is similar to that of the PAAS and UCC values, showing an upward HREE enrichment, Lu depletion, Y upward, negative Ce anomaly (δCe), and positive Eu anomaly (δEu) in dolomite-2. Chondrite has an overall lower REE content than PAAS, UCC, and Seawater, which all have the highest Ce contents among the REE (Ce content of Chondrite is only less than Y), showing negative δCe. Normalization using them hides the LREE enrichment and HREE depletion trends of the samples to some extent, whereas the dolomite formation mechanism differs from shale and Chondrite and is not intrinsically closely related, but closely related to dolomitized fluids, such as seawater (Kawabe et al., 1998; Wang et al., 2009; Wang et al., 2014a; Liu et al., 2017; Xiang et al., 2020). After normalizing using average Pacific seawater, the REE of the sample showed prominent positive δCe with LREE enrichment and HREE depletion. The HREE fraction of the host rock differs significantly from the other two because of the preferential removal of HREE features caused by near- and subsurface weathering and leaching (Fig. 11E–F).

δCe is a sensitive indicator reflecting the marine redox environment because in an oxidizing condition, Ce^{3+} is converted to Ce^{4+}, and Ce^{4+} will be adsorbed as particles; therefore, a negative δCe occurs and becomes a feature of shallow seawater (after normalization of PAAS, UCC, and Chondrite) (Bau and Dulski, 1996; Webb and Kamber, 2000; Tostevin et al., 2016; Zhou et al., 2020). δCe is calculated as $\delta Ce = Ce_N/(Pr_N^2/Nd_N)$ to avoid the influence of La and Gd on Ce abundance (Lawrence et al., 2006). All samples show positive δCe after seawater normalization because the enrichment degree of Ce in marine carbonate rocks is more significant than that of its surrounding elements (La, Pr, and Nd), resulting in the calculated positive δCe. However, this also indicates seawater or seawater-like water and has been reported in numerous studies (Wang et al., 2014a; Liu et al., 2017; Xiang et al., 2020). A good relationship occurs between the δCe anomaly and δPr ($2Pr_N/(Ce_N + Nd_N)$) (Shields and Stille, 2001). The negative δPr indicates that the positive δCe is the actual anomaly relative to seawater (Fig. 12). The host rock, dolomite-1, and dolomite-2 of the Ediacaran Dengying Formation all have positive mean δCe values of 4.601, 3.836, and 4.166, respectively (Table S). The in-situ testing of a single mineral reveals a mean δCe of 3.53 for dolomite-2, which might be more representative. The decrease in δCe reflects that the oxidation degree of dolomite-1 and dolomite-2 is greater than that of the host rock during the formation period, which might be accompanied by the mixing disturbance of deep fluid.

Positive δEu ($Eu_N/(Sm_N^2 + Tb_N)^{1/3}$, Lawrence et al., 2006) were

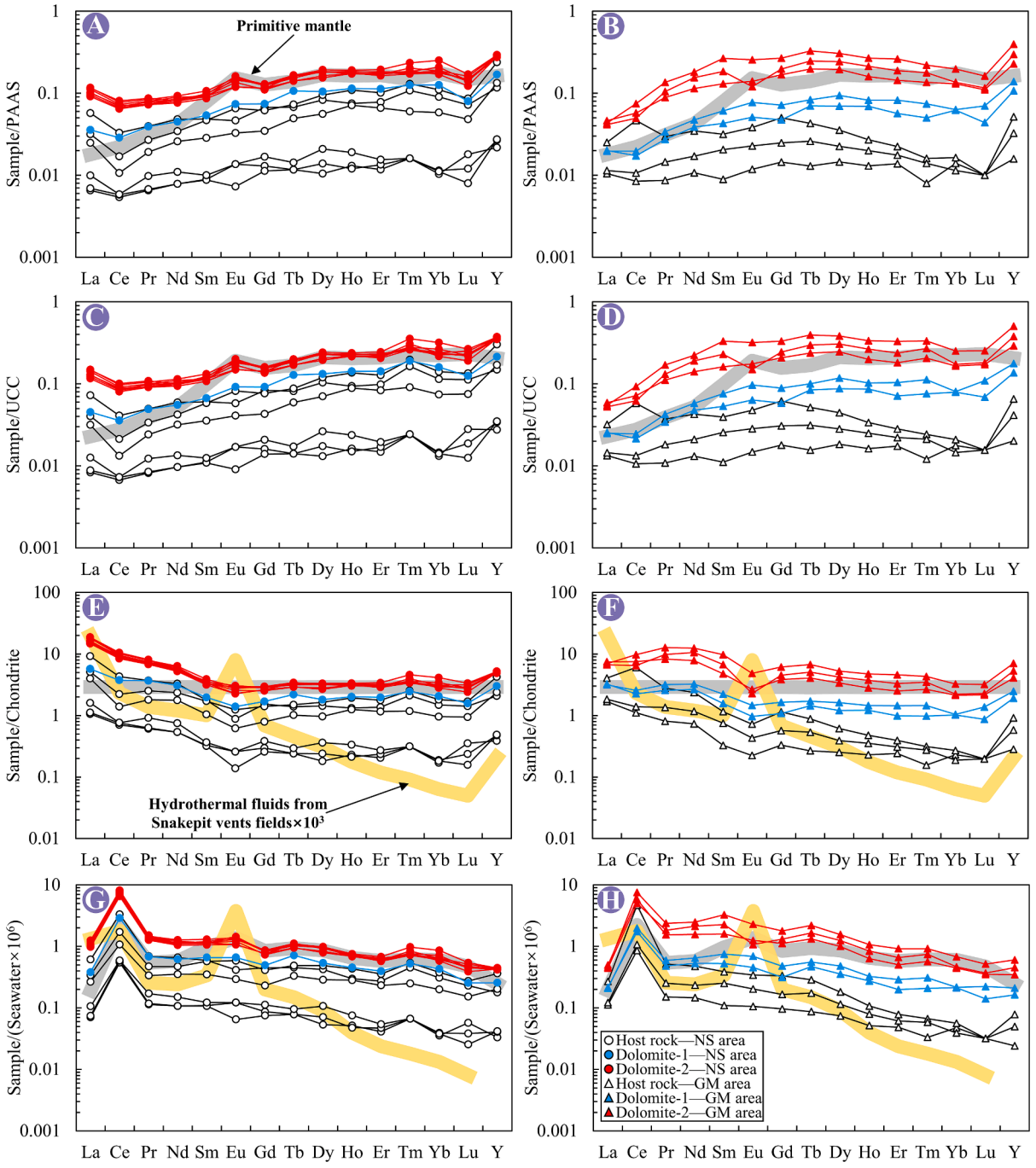

Fig. 11. REE patterns normalized to PAAS (A–B), UCC(C–D), Chondrite(E–F), and seawater(G–H) of the Ediacaran Dengying Formation in the GM and NS areas, central Sichuan Basin. Data of the Post-Archean Australian Shale (PAAS) were sourced from Taylor and McLennan (1985), the Upper Continental Crust (UCC) was sourced from McLennan (2001), the Chondrite and primitive mantle were sourced from Sun and McDonough (1989), the average Pacific seawater was sourced from Kawabe et al. (1998) and Tepe and Bau (2016), and the hydrothermal fluids from Snakepit vents fields were sourced from Douville et al. (1999; 2002).

frequently found in extremely reducing conditions or thermal fluids because Eu has two valence states of Eu^{2+} and Eu^{3+}, and Eu^{2+} is more stable at high temperatures, such as metamorphic and deep thermal fluids. Eu^{2+} can replace Ca^{2+} and enter the carbonate lattice. For example, the hydrothermal fluids from the Snakepit vents fields can reach a δEu value of 14.59 (calculated using the data from Douville et al. (1999; 2002)). The average δEu values of the host rock, dolomite-1, and dolomite-2 of the Ediacaran Dengying Formation are 0.959, 0.964, and 1.002, respectively. δEu in some dolomite-2 in-situ tests can exceed 2.0, up to 6.2 (Fig. 5H, M, R), significantly greater than dolomite-1. The PAAS normalized results are 1.07, 1.08, and 1.12, respectively. The sample shows a negative δEu, indicating that the fluid in the formation period was seawater, whereas a positive δEu indicates a contribution of deep thermal fluid. The gradual increase in δEu indicates that the temperature during the dolomite formation gradually rises. The Th of the inclusion in dolomite-2 is significantly greater than that in dolomite-1, proving that dolomite-2 was formed under higher temperatures. High Th inclusions are trapped and have dispersed salinity values. Related chronological data for this type of dolomite have been published, such as 259.4 ± 3 Ma (Su et al., 2022), while the age of fine–medium crystalline dolomite is 482 ± 14 Ma ~416 ± 23 Ma (Shen et al, 2021), and the burial depth is greater than 1000 m (Fig. 1C). Due to the uplift and

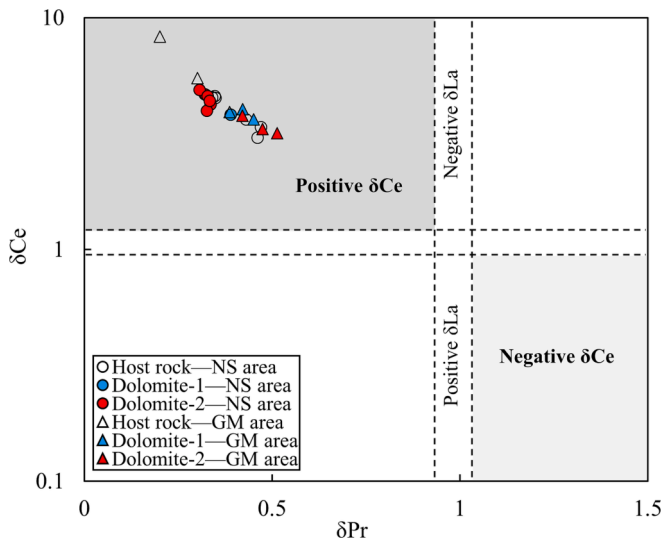

Fig. 12. The correlation diagram between the Ce anomaly (δCe) and Pr anomaly (δPr) of the Ediacaran Dengying Formation in the GM and NS areas, central Sichuan Basin. The baseline reference is from Bau and Dulski (1996).

denudation movements at the end of the Silurian, the burial depth of the Dengying Formation is less than 1000 m, and the formation temperature is far less than 80 °C (Fig. 1C), suitable for biodegradation (Head et al., 2003). This bitumen-1 is believed to be formed by biodegradation and oxidation of early reservoir oil during the Caledonian Movement and is further confirmed by the pronounced baseline hump (unresolved complex mixture) of its total ion chromatogram (Yuan, 2008; Yuan et al., 2014; Shen et al., 2021). Petrology shows that dolomite-1 was formed earlier than bitumen-1, so the age of dolomite-1 must be earlier than the oil generation and uplift period (ca. 420 Ma), where the burial depth is less than 2500 m (Fig. 1C). Furthermore, the inclusions of dolomite-1 with significantly lower Th value than that in dolomite-2, which also indicates that dolomite-1 was formed earlier than dolomite-2, belonging to shallow and deep burial stages, respectively. Simultaneously, petrological characteristics also depict that dolomite-2 was formed earlier than bitumen-2 and that bitumen-2 was derived from paleo-oil in the Late Permian–Early Triassic period (Zhu et al., 2015; Zou et al., 2015; Li et al., 2017; Su et al., 2022). Therefore, the formation temperature during the dolomite-2 stage must not exceed 200 °C. This result suggests the influence of deep thermal fluids, although the maximum temperature of the fluid itself is unknown, and a possible superposition of late burial high-temperature alterations, consistent with the incorporation of highly radiogenic Sr-containing fluids.

5.3. Formation mechanism of the Ediacaran dolomite

5.3.1. Near-surface stage

The strata of the Ediacaran Dengying Formation in the Sichuan Basin gradually began to form and develop during the Ediacaran. During this period, the central Sichuan Basin comprised an intracratonic rift and platform, with a shallow water carbonate platform in the GM and NS areas, which gradually transformed into a slope and basin facies toward the northwest (Zhao et al., 2022). The aragonite–dolomite sea dominated the upper Yangtze seawater in this period (Zhao et al., 2021), and such seawater conditions differed considerably from present-day seawater. They had high Mg/Ca ratios (lower concentrations of Mg and Ca carried by the atmosphere) and alkalinity, which was conducive to forming carbonate under early low-temperature conditions. The Precambrian dolomite sea was transient, primarily occurring during the DY2 period. Subsequently, the Mg/Ca ratio of the seawater decreased (Zhao et al., 2021), resulting in a short dolomite sea environment. In the dolomite sea environment, the fibrous dolomite can be precipitated directly, and this texture indicates the dolomite sea environment (Zhao et al., 2021; Lu et al., 2023). The DY2 reservoir rocks were characterized by grape-like and radial fibrous textures, different from the DY4 reservoir (Qian et al., 2017; Zhao et al., 2021; Lu et al., 2023). Therefore, the effect of the dolomite sea might be more crucial in the DY2 stage but was significantly weaker in the DY4 stage than other factors. In early host rock formations, numerous algae (such as cyanobacteria) on the platform will exist with carbonate sediments after death. The algae decompose and consume the dissolved oxygen in the water, speeding up the water mass reduction. Sulfate-reducing bacteria and oxygen-eating microorganisms can decompose these organic materials to promote the diagenetic replacement of a magnesian calcite precursor, promoting dolomite precipitation (Baldermann et al., 2015). This process can consume SO_4^{2-} in the water mass and release Mg^{2+} (Wang et al., 2010), improving the Mg/Ca ratio of seawater. The high Mg/Ca ratio and anoxic water (positive δCe, pyrite occasionally seen on the host rock surface, Fig. 2C) are conducive to carbonate during this period. Microorganisms make stromatolites, and algal clots of the original sedimentary texture exist in the present-day reservoir. This property is well-preserved, even though the alteration during burial was superimposed later. During the Ediacaran period, the dry arid climate in the central Sichuan Basin could have caused the evaporation and concentration of the water in the platform (Zhang et al., 2014b; Jin et al., 2019). When the evaporation intensity is high, the normal seawater on the platform is released into the atmosphere, and capillary action occurs, forming rocks with high mud contents. Seawater continuously replenishes high-salinity areas, forming a capillary cycle. Under this high-salinity evaporation, saltwater or surface water and aragonite are transformed, forming nonideal dolomite (small particle size, mud crystal, or powder crystal). Furthermore, the saltwater remaining in the high part of the platform will flow back and permeate downward under gravity (Fig. 13). Reflux dolomitization occurs when it passes through the lower high-energy beach sediments, characterized by algal dolomites and typically retains algal chutes. The dolomite crystal is fine, showing gray or dark gray, confirmed by the $^{87}Sr/^{86}Sr$ characteristics of the host rock close to the coeval seawater. Simultaneously, it has a C–O isotope background value closest to the Precambrian seawater, although it has undergone some fractional alteration.

5.3.2. Burial stage

When the buried depth is closer to and greater than 1000 m, the formation temperature increases gradually, and dolomite-1 is formed, corresponding to the shallow burial stage. In the burial stage, the compaction of the basin gradually increased, seawater and Mg^{2+}-rich saline migrated to the early host rock, and buried dolomitization occurred. Mg^{2+} will replace the Ca^{2+} in the fluid, forming dolomite with a high ordering degree. These dolomites will have lower $\delta^{18}O_{VPDB}$ values than the host rock, and the average ordering degree of dolomite-1 is 0.76, which is greater than the host rock. The mineral characteristics are still anhedral, and the mean Mg/Ca ratio is 0.78, slightly less than that of dolomite-2 (0.80). The $^{87}Sr/^{86}Sr$ value is slightly higher than that of the Precambrian seawater, indicating the mixed contribution of deep-formation saline. With further burial, the Ediacaran Dengying Formation gradually entered the deep burial stage. Here, medium- to coarse-grained dolomites are formed with a high degree of euhedral because there is enough free space and conditions for growth.

With the increase in ground stress, the dolomitization fluids here are primarily deep-formation saline and deep thermal fluids, which can up flow along fractures and faults and are rich in radiogenic Sr. It makes the present-day dolomite-2 with higher $^{87}Sr/^{86}Sr$ values and can provide numerous Mg^{2+}. Due to the high formation temperature and the support of thermal fluid, the dynamic conditions of dolomite formation are easily satisfied, therefore, the formation rate of dolomite-2 is fast. There are many strike-slip faults in the central Sichuan Basin, primarily near EW and NW trending. The fault dip is close to 90°, and the bottom is connected to the basement strata. The vertical fault displacement is the

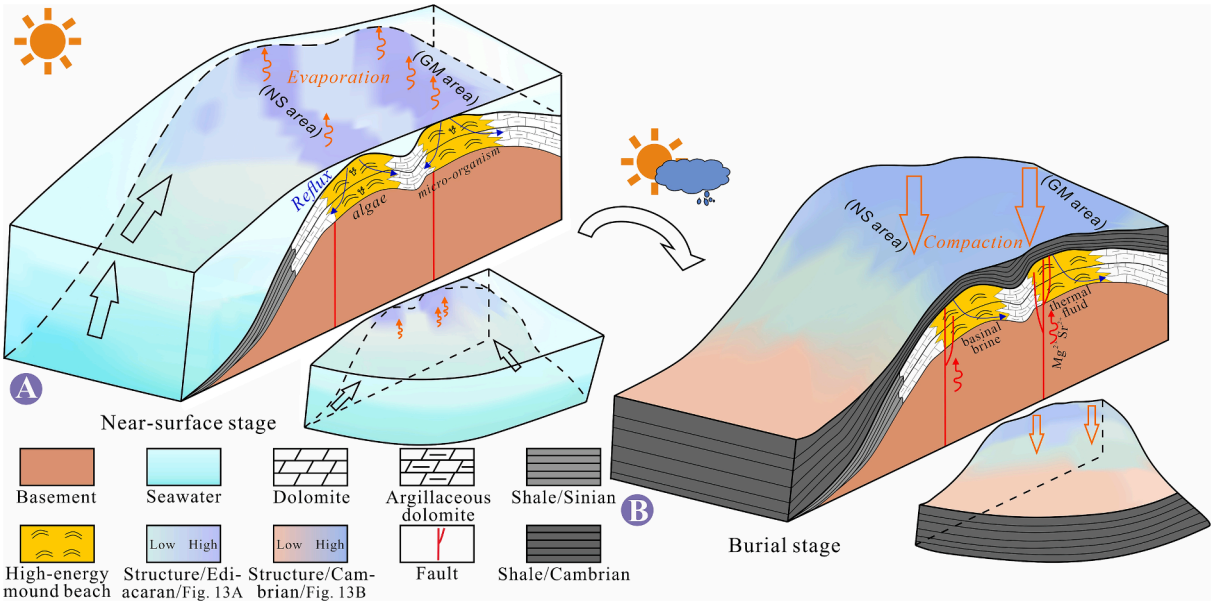

Fig. 13. The genetic model of dolomite of the Ediacaran Dengying Formation in the GM and NS areas, central Sichuan Basin.

largest in the Cambrian strata, and it gradually decreases until it disappears in the Permian strata (Ma et al., 2018; Jiao et al., 2022), reflecting the weakening fault activity. The cap rock of the Ediacaran Dengying Formation reservoir was the Qiongzhusi shale, fine-grained sediments of the Early Cambrian transgression, which was distributed throughout the central Sichuan Basin, with a thickness of 150 m to 700 m and a displacement pressure of 30–40 Ma (Li et al., 2022), providing favorable conditions for generating a restricted fluid compartment (Fig. 13). The deep fluid can flow laterally for a specific distance after encountering the top sealing, which is conducive to forming large-scale dolomite-2. Even today, the formation pressure, natural gas properties, and formation water properties above and below this barrier differ (Wu et al., 2014; Xie et al., 2021; Wei et al., 2022). Specifically, the Ediacaran Dengying Formation reservoir is a normal pressure system (pressure coefficient of 1.0–1.2), whereas the Cambrian reservoir is an abnormal overpressure system (pressure coefficient of 1.51–1.7). The Cambrian gas reservoir (avg. –32.8‰) has a smaller ethane carbon isotope value than the Ediacaran Dengying Formation (avg. –28.8‰). The average salinity of Cambrian formation water is 50.7 g/L, whereas that of the Ediacaran Dengying Formation is 123.38 g/L. Dolomite-2 has a light $\delta^{18}O_{VPDB}$ value, typically less than −10‰, due to the high-temperature alteration. The mist-centered bright-edge structures with bright red under CL, light–dark transitions, and positive δEu indicate deep-basinal brine and deep thermal fluid.

5.4. Relationship between the dolomitization process and reservoir quality

The Ediacaran Dengying Formation contains considerable natural gas resources, primarily in the remaining effective space after being filled with various dolomite, quartz minerals, and reservoir bitumen. The highest-quality reservoirs were distributed in the platform margin zone adjacent to the rift trough (Xu et al., 2021; Yang et al., 2022), reflected by high thickness and porosity. During the near-surface period, thick-layered Ediacaran microbial-algal mound beaches formed on a large scale under an arid climate and periodic seawater turbulence. In the host rock, micritic dolomite occurs under weak hydrodynamic conditions, as well as microbial action and framework, crucial to forming the original high porosity reservoir. Furthermore, the overlying strata had almost no compaction, and approximately 80% of the pores were formed during this period (Hu et al., 2020). After the primary deposition at the near-surface stage, the Tongwan-II movement occurred (Fig. 1B–C), partially eroding the mound and shoal beach at the top of the Ediacaran Dengying Formation and then large-scale karstification. Due to the limited vertical effect of karst, high-quality reservoirs are primarily within a specific depth range close to the unconformity interface. At this stage, the pore space is the largest, and the highest porosity might be close to 40% (Shen et al., 2021). Subsequently, the Ediacaran reservoirs experienced shallow and deep burial stages, and dolomite-1 and dolomite-2 began to form in the original high-quality reservoirs, which largely occupied the preexisting space of the reservoir. Deep thermal fluid channeled by faults contributed to the formation of dolomite-2. These fluids were typically weakly acidic and could have dissolved the preexisting pores and made them have a harbor-like shape (Fig. 3L). However, precipitation typically occurs after a low degree of dissolution, forming dolomite-2 with larger crystals. Furthermore, the compaction of the overlying strata is intensified, weakening its construction effect on the reservoir. Therefore, the host rock formation and karst reconstruction in the Tongwan movement are the most critical factors for developing effective reservoirs in the deeply buried Ediacaran Dengying Formation. The water energy conditions of the platform margin are high in the near-surface stage, therefore, the proportion of the thickness with a porosity of 2–5% decreases from the platform margin to the intraplatform, for example, from well MX9 (29%) to wells MX17 (24%) and MX39 (7%). The proportion of thickness with porosity exceeding 5% also decreases (3%, 1%, and 0.4%, respectively) (Fig. 14). Due to the poor physical properties of the original reservoir, the constructive reconstruction by fluid alteration during the formation of dolomite-2 is the most crucial in the intraplatform margin.

6. Conclusions

Combined with the latest drilling coring data from the NS area, the mineral sequences and the characteristics of ancient fluids recorded by dolomite of the Ediacaran reservoir in the central Sichuan Basin were studied. The main conclusions of this study are as follows:

(1) The host rock formation is closely related to the coeval seawater, although the C–O isotope are altered and fractionated under microbial and late high-temperature conditions. The microorganisms, evaporation concentration, and reflux infiltration are essential in this stage.

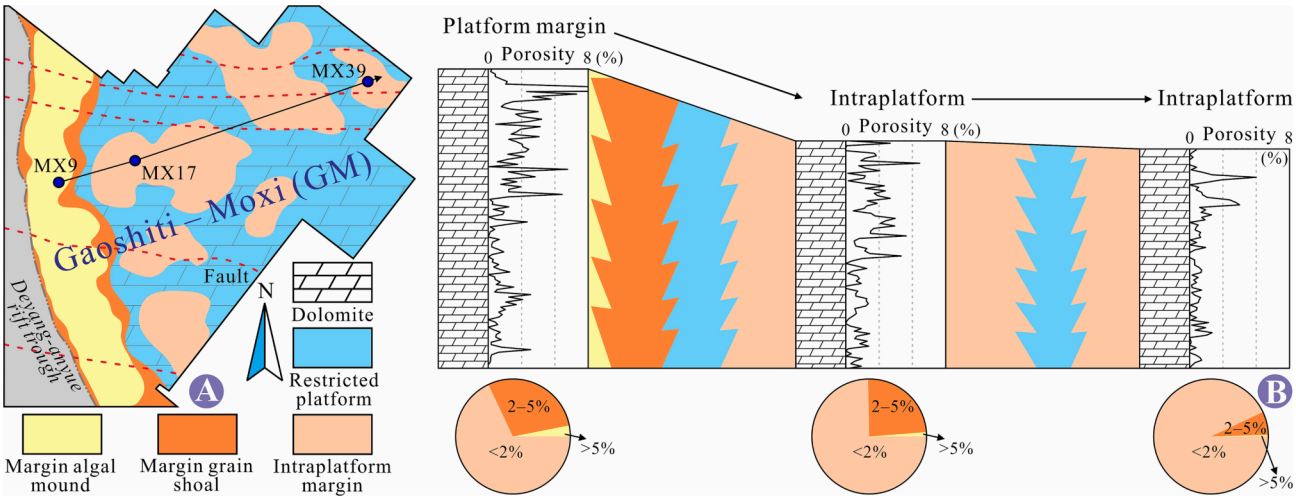

Fig. 14. Lithofacies paleogeography of the Ediacaran Dengying Formation (A) (modified after Yang et al., 2022), and thickness and porosity of the reservoir from the platform margin to intraplatform margin (B), central Sichuan Basin.

(2) The formation of dolomite-1 is the product of shallow burial, and the fluid is primarily a mixture of seawater and deep-basinal brine. However, the burial depth of dolomite-2 is large when it is formed, and the fluid is primarily deep-basinal brine and deep thermal fluid.
(3) Based on petrological research, combined with C–O–Sr isotope, the REE and some trace elements (e.g., Sr, Mn, Fe, and P) are effective for studying the fluid properties and genesis of ancient and deeply buried dolomite, whereas the ordering degree needs to be treated with caution.

CRediT authorship contribution statement

Yishu Li: Investigation, Conceptualization, Methodology, Software, Visualization, Writing – original draft. **Guangdi Liu:** Methodology, Writing – review & editing. **Zezhang Song:** Writing – review & editing. **Mingliang Sun:** Writing – review & editing. **Xingwang Tian:** Resources. **Dailing Yang:** Resources. **Yunlong Wang:** Resources. **Lianqiang Zhu:** Investigation. **Fuliang You:** Investigation.

Declaration of Competing Interest

The authors declare that they have no known competing financial interests or personal relationships that could have appeared to influence the work reported in this paper.

Data availability

Data will be made available on request.

Acknowledgements

This research was supported by the National Key R&D Program of China (Grant No. 2017YFC0603106). Special thanks to editor Ahmed E. Radwan and three anonymous reviewers for their constructive suggestions in improving the manuscript. We also sincerely thank the Research Institute of Exploration and Development, PetroChina Southwest Oil & Gas Field Company for providing samples and data.

Appendix A. Supplementary data

Supplementary data to this article can be found online at https://doi.org/10.1016/j.jseaes.2023.105780.

References

Bagrintseva, K.I., 2015. Carbonate reservoir rocks. John Wiley & Sons.
Bahnan, A.E., Pironon, J., Carpentier, C., Barre, G., Gaucher, E.G., 2021. The diagenetic history of the giant Lacq gas field, witness to the apto-albian rifting and the Pyrenean orogeny, revealed by fluid and basin modeling. Mar. Pet. Geol. 133, 405250 https://doi.org/10.1016/j.marpetgeo.2021.105250.
Bai, Y., Liu, W., Xu, W.L., 2022. Dolomite genesis and dolomitization mechanisms of the Ordovician lower Yingshan Formation, Gucheng area, Tarim Basin, China. J. Pet. Sci. Eng. 215, 110570 https://doi.org/10.1016/j.petrol.2022.110570.
Baldermann, A., Deditius, A.P., Dietzel, M., Fichtner, V., Fischer, C., Hippler, D., Leis, A., Baldermann, C., Mavromatis, V., Stickler, C.P., Strauss, H., 2015. The role of bacterial sulfate reduction during dolomite precipitation: implications from Upper Jurassic platform carbonates. Chem. Geol. 412, 1–14. https://doi.org/10.1016/j.chemgeo.2015.07.020.
Baniak, G.M., Amskold, L., Konhauser, K.O., Muehlenbacks, K., Pemberton, S.G., Gingras, M.K., 2014. Sankha and burrow-mediated dolomitization in the Mississippian Debolt Formation, Northwestern Alberta. Canada. Ichnos. 21, 158–174. https://doi.org/10.1080/10420940.2014.930036.
Barbosa, L.C., Nascimento, M., Araújo, O., Medeiros, J.D., 2020. A cleaner and more sustainable decarbonation process via ionic-liquid absorption for natural gas with high carbon dioxide content. J. Clean. Prod. 242, 118421 https://doi.org/10.1016/j.jclepro.2019.118421.
Bau, M., Dulski, P., 1996. Distribution of yttrium and rare-earth elements in the Penge and Kuruman iron-formations, Transvaal Supergroup. South Africa. Precambrian Research. 79, 37–55. https://doi.org/10.1016/0301-9268(95)00087-9.
Bhat, G.M., Craig, J., Hafiz, M., Hakhoo, N., Thurow, J.W., Thusu, B., Cozzi, A., 2012. Geology and hydrocarbon potential of Neoproterozoic-Cambrian Basins in Asia: an introduction. Geol. Soc. Lond. Spec. Publ. 366, 1–17. https://doi.org/10.1144/SP366.15.
Bodnar, R.J., 1993. Revised equation and table for determining the freezing point depression of H_2O–Nacl solutions. Geochim. Cosmochim. Acta 57, 683–684. https://doi.org/10.1016/0016-7037(93)90378-A.
Bruguier, O., Caby, R., Bosch, D., Ouzegane, K., Deloule, E., Dhuime, B., Bendaoud, A., Kienast, J.R., 2020. A case study of in situ analyses (major and trace elements, U-Pb geochronology and Hf–O isotopes) of a zircon megacryst: Implication for the evolution of the Egere terrane (Central Hoggar, Tuareg Shield, Algeria). Precambr. Res. 351, 105966 https://doi.org/10.1016/j.precamres.2020.105966.
Burns, S.J., Haudenschild, U., Matter, A., 1994. The strontium isotopic composition of carbonates from the late Precambrian (~ 560–540 Ma) Huqf Group of Oman. Chem. Geol. 111, 269–282. https://doi.org/10.1016/0009-2541(94)90094-9.
Chen, Y.N., Shen, A.J., Pan, L.Y., Zhang, J., Wang, X.F., 2017. Features, origin and distribution of microbial dolomite reservoirs: A case study of 4th Member of Sinian Dengying Formation in Sichuan Basin. SW China. Petroleum Exploration and Development. 44, 745–757. https://doi.org/10.1016/S1876-3804(17)30085-X.
Craig, J., Thurow, J., Thusu, B., Whitham, A., Abutarruma, Y., 2009. Global Neoproterozoic petroleum systems: The emerging potential in North Africa. Geol. Soc. Lond. Spec. Publ. 326, 1–25. https://doi.org/10.1144/SP326.1.
Craig, J., Grigo, D., Rebora, A., Serafini, G., Tebaldi, E., 2010. From Neoproterozoic to Early Cenozoic: Exploring the potential of older and deeper hydrocarbon plays across North Africa and the Middle East. Geological Society, London, Petroleum Geology Conference Series. 7, 673–705. https://doi.org/10.1144/0070673.
Craig, J., Biff, U., Galimberti, R.F., Ghori, K.A.R., Gorter, J.D., Hakhoo, N., Heron, D.P.L., Thurow, J., Vecoli, M., 2013. The palaeobiology and geochemistry of Precambrian hydrocarbon source rocks. Mar. Pet. Geol. 40, 1–47. https://doi.org/10.1016/j.marpetgeo.2012.09.011.

Douville, E., Bienvenu, P., Charlou, J.L., Donval, J.P., Fouquet, Y., Appriou, P., Gamo, T., 1999. Yttrium and rare earth elements in fluids from various deep-sea hydrothermal systems. Geochim. Cosmochim. Acta 63, 627–643. https://doi.org/10.1016/S0016-7037(99)00024-1.

Douville, E., Charlou, J.L., Oelkers, E.H., Bienvenu, P., Colon, C.F.J., Donval, J.P., Fouquet, Y., Prieur, D., Appriou, P., 2002. The rainbow vent fluids (36°14′N, MAR): the influence of ultramafic rocks and phase separation on trace metal content in Mid-Atlantic Ridge hydrothermal fluids. Chem. Geol. 184, 37–48. https://doi.org/10.1016/S0009-2541(01)00351-5.

Dyman, T.S., Crovelli, R.A., Bartberger, C.E., Takahashi, K.I., 2002. Worldwide estimates of deep natural gas resources based on the U.S. geological survey world petroleum assessment 2000. Nat. Resour. Res. 11, 207–218. https://doi.org/10.1023/A:1019860722244.

Dyman, T.S., Wyman, R.E., Kuuskraa, V.A., Lewan, M.D., Cook, T.A., 2003. Deep natural gas resources. Nat. Resour. Res. 12, 41–56. https://doi.org/10.1023/A:1022656421803.

Fairchild, I.J., Spencer, A.M., Ali, D.O., Anderson, R.P., Anderton, R., Boomer, I., Dove, D., Evans, J.D., Hambrey, M.L., Howe, J., Sawaki, Y., Shields, G.A., Skelton, A., Tucker, M.E., Wang, Z.R., Zhou, Y., 2018. Tonian-Cryogenian boundary sections of Argyll. Scotland. Precambrian Research. 319, 37–64. https://doi.org/10.1016/j.precamres.2017.09.020.

Fairchild, I.J., Spiro, B., 1987. Petrological and isotopic implications of some contrasting Late Precambrian carbonates, NE Spitsbergen. Sedimentology 34, 973–989. https://doi.org/10.1111/j.1365-3091.1987.tb00587.x.

Feng, Z.Z., Jin, Z.K., 1994. Types and origin of dolostones in the Lower Palaeozoic of the North China Platform. Sed. Geol. 93, 279–290. https://doi.org/10.1016/0037-0738(94)90011-6.

Feng, M.Y., Wu, P.C., Qiang, Z.T., Liu, X.H., Duan, Y., Xia, M.L., 2017. Hydrothermal dolomite reservoir in the Precambrian Dengying Formation of central Sichuan Basin. Southwestern China. Marine and Petroleum Geology. 82, 206–219. https://doi.org/10.1016/j.marpetgeo.2017.02.008.

Friedman, G.M., Sanders, J., 1967. Origin and Occurrence of Dolostones. Dev. Sedimentol. 9, 267–348. https://doi.org/10.1016/S0070-4571(08)71114-2.

Frolov, S.V., Akhmanov, G.G., Bakay, E.A., Lubnina, N.V., Korobova, N.I., Karnyushina, E.E., Kozlova, E.V., 2015. Meso-Neoproterozoic petroleum systems of the Eastern Siberian sedimentary basins. Precambr. Res. 159, 95–113. https://doi.org/10.1016/j.precamres.2014.11.018.

Gao, P., Liu, G.D., Lash, G.G., Li, B.Y., Yan, D.T., Chen, C., 2018. Occurrences and origin of reservoir solid bitumen in Sinian Dengying Formation dolomites of the Sichuan Basin, SW China. Int. J. Coal Geol. 200, 135–152. https://doi.org/10.1016/j.coal.2018.11.001.

Goldsmith, T.R., Graf, D.L., 1958. Structural and compositional variations in some natural dolomites. J. Geol. 66, 678–693. https://doi.org/10.1086/626547.

Guido, A., Russo, F., Miriello, D., Mastandrea, A., 2018. Autochthonous micrite to aphanodolomite: the microbialites in the dolomitization processes. Geosciences 8, 451. https://doi.org/10.3390/geosciences8120451.

Ha, Y.J., Kumar, M.S., Park, K.H., Song, Y.S., Liu, S.W., 2021. Carbon, oxygen and strontium isotope geochemistry of the late Neoproterozoic carbonate platform deposit Hyangsanni dolomite of the Okcheon metamorphic belt. Korea. Lithos. 396–397, 106219 https://doi.org/10.1016/j.lithos.2021.106219.

Halverson, G.P., Dudás, F.Ö., Maloof, A.C., Bowring, S.A., 2007. Evolution of the $^{87}Sr/^{86}Sr$ composition of Neoproterozoic seawater. Palaeogeogr. Palaeoclimatol. Palaeoecol. 256, 103–129. https://doi.org/10.1016/j.palaeo.2007.02.028.

Head, I.M., Jones, D.M., Larter, S.R., 2003. Biological activity in the deep subsurface and the origin of heavy oil. Nature 426, 344–352. https://doi.org/10.1038/nature02134.

Hemming, N.G., Meyers, W.J., Grams, J.C., 1989. Cathodoluminescence in diagenetic calcites: the role of Fe and Mn as deduced from electron probe and spectrophotometric measurements. J. Sediment. Res. 59, 404–411. https://doi.org/10.1306/212F8FA8-2B24-11D7-8648000102C1865D.

Hoffman, P.F., Kaufman, A.J., Halverson, G.P., Schrag, D.P., 1998. A Neoproterozoic Snowball Earth. A Neoproterozoic Snowball Earth. Science. 281 (5381), 1342–1346.

Hsü, K.J., Schneider, C.S., 1973. Progress report on dolomitization-hydrology of Abu Dhabi Sabkhas, Arabian Gulf. Springer, Berlin, pp. 409–422.

Hu, Y.J., Cai, C.F., Pederson, C.L., Liu, D.W., Jiang, L., He, X.Y., Shi, S.Y., Immenhauser, A., 2020. Dolomitization history and porosity evolution of a giant, deeply buried Ediacaran gas field (Sichuan Basin, China). Precambr. Res. 338, 105595 https://doi.org/10.1016/j.precamres.2020.105595.

Huang, B.W., Zhang, S.N., Lu, Z.Y., Ye, N., Zhu, B., Ding, X.Q., Li, Y.T., 2021. Origin of dolomites in Lower-Middle Ordovician carbonate rocks in the Yingshan Formation, Gucheng Area, Tarim Basin: Evidence from petrography and geochemical data. Mar. Pet. Geol. 134, 105322 https://doi.org/10.1016/j.marpetgeo.2021.105322.

Jia, C.Z., Pang, X.Q., 2015. Research processes and main development directions of deep hydrocarbon geological theories. Acta Pet. Sin. 36, 1457–1469 in Chinese.

Jiang, Y.Q., Tao, Y.Z., Gu, Y.F., Wang, Y.B., Qiang, Z.T., Jiang, N., Lin, G., Jiang, C., 2016. Hydrothermal dolomitization in Dengying Formation, Gaoshiti-Moxi area, Sichuan Basin. SW China. Petroleum Exploration and Development. 43, 54–64. https://doi.org/10.1016/S1876-3804(16)30006-4.

Jiao, F.Z., Yang, Y., Ran, Q., Wu, G.H., Liang, H., 2022. Distribution and gas exploration of the strike-slip faults in the central Sichuan Basin. Nat. Gas Ind. 9, 63–72. https://doi.org/10.1016/j.ngib.2021.08.018.

Jin, M.D., Tan, X.C., Li, B.S., Zhu, X., Zeng, W., Lian, C.B., 2019. Genesis of dolomite in the Sinian Dengying Formation in the Sichuan Basin. Acta Sedimentol. Sin. 37, 443–454 in Chinese.

Kaufman, A.J., Knoll, A.H., 1995. Neoproterozoic variations in the C-isotopic composition of seawater: stratigraphic and biogeochemical implications. Precambr. Res. 73, 27–49. https://doi.org/10.1016/0301-9268(94)00070-8.

Kawabe, I., Tokahiro, T., Ohta, A., Miura, N., 1998. Monoisotopic REE abundances in seawater and the origin of seawater tetrad effect. Geochem. J. 32, 213–229. https://doi.org/10.2343/geochemj.32.213.

Kimura, H., Watanabe, Y., 2001. Oceanic anoxia at the Precambrian-Cambrian boundary. Geology 29, 995–998. https://doi.org/10.1130/0091-7613(2001)029.

Krabbenhöft, A., Eisenhauer, A., Bohm, F., Vollstaedt, H., Fiztzke, J., Liebetrau, V., Augustin, N., Ehrenbrink, B.P., Muller, M.N., Horn, C., Hansen, B.T., Nolte, N., Wallmann, K., 2010. Constraining the marine strontium budget with natural strontium isotope fractionations ($^{87}Sr/^{86}Sr^*$, $\delta^{88/86}Sr$) of carbonates, hydrothermal solutions and river waters. Geochim. Cosmochim. Acta 74, 4097–4109. https://doi.org/10.1016/j.gca.2010.04.009.

Land, L.S., 1985. The origin of massive dolomite. J. Geol. Educ. 33, 112–125. https://doi.org/10.5408/0022-1368-33.2.112.

Lawrence, M.G., Greig, A., Collerson, K.D., Kamber, B.S., 2006. Rare Earth Element and Yttrium Variability in South East Queensland Waterways. Aquat. Geochem. 12, 39–72. https://doi.org/10.1007/s10498-005-4471-8.

Li, Y., Kang, Z.J., Xue, Z.J., Zheng, S.Q., 2018. Theories and practices of carbonate reservoirs development in China. Pet. Explor. Dev. 45, 712–722. https://doi.org/10.1016/S1876-3804(18)30074-0.

Li, J., Li, Z.S., Wang, X.B., Wang, D.L., Xie, Z.Y., Li, J., Wang, Y.F., Han, Z.X., Ma, C.H., Wang, Z.H., Cui, H.Y., Wang, R., Hao, A.S., 2017. New indexes and charts for genesis identification of multiple natural gases. Pet. Explor. Dev. 44, 535–543. https://doi.org/10.1016/S1876-3804(17)30062-9.

Li, Q., Liu, G.D., Song, Z.Z., Sun, M.L., Cao, Y.S., Zhu, L.Q., Tian, X.W., Yang, D.L., Wang, Y.L., You, F.L., 2022. Analysis on preservation effectiveness of lithologic gas reservoirs in north slope of central Sichuan paleo-uplift: Case study of the second member of the Dengying Formation in Well Pengtan-1. Nat. Gas Geosci. 33, 1276–1285 in Chinese.

Liu, Y.S., Hu, Z.C., Gao, S., Günther, D., Xu, J., Gao, C.G., Chen, H.H., 2008. In situ analysis of major and trace elements of anhydrous minerals by LA-ICP-MS without applying an internal standard. Chem. Geol. 257, 34–43. https://doi.org/10.1016/j.chemgeo.2008.08.004.

Liu, C., Xie, Q.B., Wang, G.W., He, W.G., Song, Y.F., Tang, Y., Wang, Y.H., 2017. Rare earth element characteristics of the carboniferous Huanglong Formation dolomites in eastern Sichuan Basin, southwest China: Implications for origins of dolomitizing and diagenetic fluids. Mar. Pet. Geol. 81, 33–49. https://doi.org/10.1016/j.marpetgeo.2016.12.030.

Lu, P.D., Li, Z.Q., Tian, T.Z., Wu, J., Sun, W., Qiao, Z.F., Wang, Y.S., Liu, S.G., Deng, B., 2023. Research of the botryoidal-lace shape structure and its role in reservoir control in the Sinian Dengying Formation second Member of the Sichuan Basin. Earth Sci. Front. 1–19 in Chinese.

Luemba, M., Chen, Z.H., Ntibahanana, J., 2021. Molecular markers of Neoproterozoic-Lower Paleozoic petroleum systems and their geological significance: A case study of the cratonic basins in western China. J. Pet. Sci. Eng. 204, 108707 https://doi.org/10.1016/j.petrol.2021.108707.

Ma, Y.S., Cai, X.Y., Yun, L., Li, Z.J., Li, H.L., Deng, S., Zhao, P.R., 2022. Practice and theoretical and technical progress in exploration and development of Shunbei ultra-deep carbonate oil and gas field, Tarim Basin. NW China. Petroleum Exploration and Development. 49, 1–20. https://doi.org/10.1016/S1876-3804(22)60001-6.

Ma, D.B., Wang, Z.C., Duan, S.F., Gao, J.R., Jiang, Q.C., Jiang, H., Zeng, F.Y., Lu, W.H., 2018. Strike–slip faults and their significance for hydrocarbon accumulation in Gaoshiti-Moxi area, Sichuan Basin. SW China. Petroleum Exploration and Development. 45, 851–861. https://doi.org/10.1016/S1876-3804(18)30088-0.

Machel, H.G., Burton, E.A., 1991. Factors governing cathodoluminescence in calcite and dolomite, and their implications for studies of carbonate diagenesis. Luminescence Microscopy and Spectroscopy: Qualitative and Quantitative Applications. SEPM Short Course 25, 37–57.

Manche, C., Kaczmarek, S.E., 2021. A global study of dolomite stoichiometry and cation ordering through the Phanerozoic. J. Sediment. Res. 91, 520–546. https://doi.org/10.2110/jsr.2020.204.

Mattes, B.W., Mountjoy, E.W., 1980. Burial dolomitization of the Upper Devonian Miette Buildup. Jasper National Park, Alberta.

McArthur, J.M., Howarth, R.J., Bailey, T.R., 2001. Strontium isotope stratigraphy: LOWESS Version 3: best fit to the marine Sr-isotope Curve for 0–509 Ma and accompanying look-up table for deriving numerical age. J. Geol. 109, 155–170. https://doi.org/10.1086/319243.

McLennan, S.M., 2001. Relationships between the trace element composition of sedimentary rocks and upper continental crust. Geochem. Geophys. Geosyst. 2 (4) https://doi.org/10.1029/2000GC000109, 2000GC000109.

Nothdurft, L.D., Webb, G.E., Kamber, B.S., 2004. Rare earth element geochemistry of Late Devonian reefal carbonates, Canning Basin, Western Australia: Confirmation of a seawater REE proxy in ancient limestones. Geochim. Cosmochim. Acta 68, 263–283. https://doi.org/10.1016/S0016-7037(03)00422-8.

Otsuji, N., Kumar, M.S., Kamer, A., Tsuchiya, N., Kawakami, T., Ishikawa, M., Grantham, G.H., 2013. Late-Tonian to early–Cryogenian apparent depositional ages for metacarbonate rocks from the Sør Rondane Mountains. East Antarctica. Precambrian Research. 234, 257–278. https://doi.org/10.1016/j.precamres.2012.10.016.

Qian, Y.X., Feng, J.F., He, Z.L., Zhang, K.Y., Jin, T., Dong, S.F., You, D.H., Zhang, Y.D., 2017. Applications of petrography and isotope analysis of micro-drill samples to the study of genesis of grape-like dolomite of the Dengying Formation in the Sichuan Basin. Oil Gas Geol. 38, 665–676 in Chinese.

Scholle, P.A., Ulmer-Scholle, D.S., 2003. A color guide to the petrography of carbonate rocks: grains, textures, porosity, diagenesis. AAPG Mem. 77 https://doi.org/10.1306/M77973.

Shembilu, N., Azmy, K., Blamey, N., 2021. Origin of Middle-Upper Cambrian dolomites in eastern Laurentia: A case study from Belle Isle strait, western Newfoundland. Mar. Pet. Geol. 125, 104858 https://doi.org/10.1016/j.marpetgeo.2020.104858.

Shen, A.J., Zhao, W.Z., Hu, A.P., Wang, H., Liang, F., Wang, Y.S., 2021. The dating and temperature measurement technologies for carbonate minerals and their application in hydrocarbon accumulation research in the paleo-uplift in central Sichuan Basin. SW China. Petroleum Exploration and Development. 48, 555–568. https://doi.org/10.1016/S1876-3804(21)60045-9.

Shergold, J.H., Cooper, R.A., 2004. The Cambrian Period. A Geological Time Scale. 147–164 https://doi.org/10.1017/CBO9780511536045.012.

Shields, G., Stille, P., 2001. Diagenetic constraints on the use of cerium anomalies as palaeoseawater redox proxies: an isotopic and REE study of Cambrian phosphorites. Chem. Geol. 175, 29–48. https://doi.org/10.1016/S0009-2541(00)00362-4.

Sibley, D.F., Gregg, J.M., 1987. Classification of dolomite rock textures. J. Sediment. Res. 57, 967–975. https://doi.org/10.1306/212F8CBA-2B24-11D7-8648000102C1865D.

Song, W.H., 1996. Research on reservoir-formed conditions of large to medium gas fields of Leshan-Longnvsi palaeohigh. Nat. Gas Ind. 16, 13–26 in Chinese.

Steiger, R.H., Jäger, E., 1977. Subcommission on geochronology: Convention on the use of decay constants in geo- and cosmochronology. Earth Planet. Sci. Lett. 36, 359–362. https://doi.org/10.1016/0012-821X(77)90060-7.

Su, A., Chen, H.H., Feng, Y.X., Zhao, J.X., Wang, Z.C., Hu, M.Y., Jiang, H., Nguyen, A.D., 2022. In situ U-Pb dating and geochemical characterization of multi-stage dolomite cementation in the Ediacaran Dengying Formation, Central Sichuan Basin, China: Constraints on diagenetic, hydrothermal and paleo-oil filling events. Precambr. Res. 368, 106481 https://doi.org/10.1016/j.precamres.2021.106481.

Sun, S.S., McDonough, W.F., 1989. Chemical and isotopic systematics of oceanic basalts: implications for mantle composition and processes. Geological Society of London Special Publications. 42, 313–345. https://doi.org/10.1144/GSL.SP.1989.042.01.19.

Sun, L.D., Zou, C.N., Zhu, R.K., Zhang, Y.H., Zhang, S.C., Zhang, B.M., Zhu, G.Y., Gao, Z. Y., 2013. Formation, distribution and potential of deep hydrocarbon resources in China. Pet. Explor. Dev. 40, 687–695. https://doi.org/10.1016/S1876-3804(13)60093-2.

Taylor, S.R., McLennan, S.M., 1985. The continental crust: Its composition and evolution. Blackwell Scientific Publication, Oxford, p. 312.

Tepe, N., Bau, M., 2016. Behavior of rare earth elements and yttrium during simulation of arctic estuarine mixing between glacial-fed river waters and seawater and the impact of inorganic (nano-)particles. Chem. Geol. 438, 134–145. https://doi.org/10.1016/j.chemgeo.2016.06.001.

Tostevin, R., Shields, G.A., Tarbuck, G.M., He, T.C., Clarkson, M.O., Wood, R.A., 2016. Effective use of cerium anomalies as a redox proxy in carbonate-dominated marine settings. Chem. Geol. 438, 146–162. https://doi.org/10.1016/j.chemgeo.2016.06.027.

Vasconcelos, C., McKenzie, J.A., 1997. Microbial mediation of modern dolomite precipitation and diagenesis under anoxic conditions (Lagoa Vermelha, Rio de Janeiro, Brazil). J. Sediment. Res. 67, 378–390. https://doi.org/10.1306/D4268577-2B26-11D7-8648000102C1865D.

Wang, X.L., Hu, W.X., Chen, Q., Li, Q., Zhu, J.Q., Zhang, J.T., 2010. Characteristics and formation mechanism of upper Sinian algal dolomite at the Kepin area, Tarim Basin. NW China. Acta Geologica Sinica. 84, 1479–1494 in Chinese.

Wang, L.C., Hu, W.X., Wang, X.L., Cao, J., Chen, Q., 2014a. Seawater normalized REE patterns of dolomites in Geshan and Panlongdong sections, China: Implications for tracing dolomitization and diagenetic fluids. Mar. Pet. Geol. 56, 63–73. https://doi.org/10.1016/j.marpetgeo.2014.02.018.

Wang, H.G., Huang, H.C., Bi, W.X., Ji, G.D., Zhou, B., Zhuo, L.B., 2022. Deep and ultra-deep oil and gas well drilling technologies: Progress and prospect. Nat. Gas Ind. 9, 141–157. https://doi.org/10.1016/j.ngib.2021.08.019.

Wang, Z.C., Jiang, H., Wang, T.S., Lu, W.H., Gu, Z.D., Xu, A.N., Yang, Y., Xu, Z.H., 2014b. Paleo-geomorphology formed during Tongwan tectonization in Sichuan Basin and its significance for hydrocarbon accumulation. Pet. Explor. Dev. 41, 338–345. https://doi.org/10.1016/S1876-3804(14)60038-0.

Wang, X.L., Jin, Z.J., Hu, W.X., Zhang, J.T., Qian, Y.X., Zhu, J.Q., Li, Q., 2009. Using in situ REE analysis to study the origin and diagenesis of dolomite of Lower Paleozoic, Tarim Basin. Sci China Ser D Earth Sci 52, 681–693. https://doi.org/10.1007/s11430-009-0057-4.

Warren, J., 2000. Dolomite: occurrence, evolution and economically important associations. Earth Sci. Rev. 52, 1–81. https://doi.org/10.1016/S0012-8252(00)00022-2.

Warthmann, R., Lith, Y.V., Vasconcelos, C., McKenzie, J.A., Karpoff, A.M., 2000. Bacterially induced dolomite precipitation in anoxic culture experiments. Geology 28, 1091–1094. https://doi.org/10.1130/0091-7613(2000)28<1091:BIDPIA>2.0.CO;2.

Webb, G.E., Kamber, B.S., 2000. Rare earth elements in Holocene reefal microbialites: a new shallow seawater proxy. Geochim. Cosmochim. Acta 64, 1557–1565. https://doi.org/10.1016/S0016-7037(99)00400-7.

Wei, G.Q., Xie, Z.Y., Yang, Y., Li, J., Yang, W., Zhao, L.Z., Yang, C.L., Zhang, L., Xie, W.R., Jiang, H., Li, Z.S., Li, J., Guo, J.Y., 2022. Formation conditions of Sinian-Cambrian large lithologic gas reservoirs in the north slope area of central Sichuan Basin. SW China. Petroleum Exploration and Development. 49, 963–976. https://doi.org/10.1016/S1876-3804(22)60325-2.

Wierzbicki, R., Dravis, J.J., Al-Aasm, I., Harland, N., 2006. Burial dolomitization and dissolution of Upper Jurassic Abenaki platform carbonates, Deep Panuke reservoir, Nova Scotia. Canada. AAPG Bulletin. 90, 1843–1861. https://doi.org/10.1306/03200605074.

Wu, J., Liu, S.G., Zhao, Y.H., Sun, W., Song, L.K., Song, J.M., Liang, F., Tian, Y.H., Long, Y., Li, J.L., 2014. Fluid characteristics of Upper Sinian-Lower Cambrian petroliferous strata in Gaoshiti-Moxi structure of Sichuan Basin, China. Journal of Chengdu University of Technology. 41, 713–722 in Chinese.

Xiang, P.F., Ji, H.C., Shi, Y.Q., Huang, Y., Sun, Y.S., Xu, X.R., Zou, S.Q., 2020. Petrographic, rare earth elements and isotope constraints on the dolomite origin of Ordovician Majiagou Formation (Jizhong Depression, North China). Mar. Pet. Geol. 117, 104374 https://doi.org/10.1016/j.marpetgeo.2020.104374.

Xie, Z.Y., Li, J., Yang, C.L., Tian, X.W., Zhang, L., Li, J., Li, Z.S., Guo, J.Y., Xie, W.R., Guo, Z.Q., Qi, X.N., Hao, A.S., 2021. Geochemical characteristics of Sinian-Cambrian natural gas in central Sichuan paleo-uplift and exploration potential of Taihe gas area. Nat. Gas Ind. 41, 1–14 in Chinese.

Xu, C.C., Shen, P., Yang, Y.M., Zhao, L.Z., Luo, B., Wen, L., Chen, K., Ran, Q., Zhong, Y., Peng, H.L., 2021. New understandings and potential of Sinian-Lower Paleozoic natural gas exploration in the central Sichuan paleo-uplift of the Sichuan Basin. Nat. Gas Ind. 8, 105–113. https://doi.org/10.1016/j.ngib.2020.07.007.

Yang, X.Y., Mei, Q.Y., Wang, X.Z., Dong, Z.X., Li, Y., Huo, F., 2018a. Indication of rare earth element characteristics to dolomite petrogenesis-A case study of the fifth member of Ordovician Majiagou Formation in the Ordos Basin, central China. Mar. Pet. Geol. 92, 1028–1040. https://doi.org/10.1016/j.marpetgeo.2017.12.004.

Yang, Y., Wang, Z.C., Wen, L., Xie, W.R., Fu, X.D., Li, W.Z., 2022. Sinian hydrocarbon accumulation conditions and Exploration potential at the northwest margin of the Yangtze region. China. Petroleum Exploration and Development. 49, 272–284. https://doi.org/10.1016/S1876-3804(22)60023-5.

Yang, Y.M., Yang, Y., Yang, G., Song, J.R., Wen, L., Deng, C.G., Xia, M.L., Ran, Q., Duan, G.B., Luo, B., Xie, B., 2018b. Gas accumulation conditions and key technologies for exploration & development of Sinian and Cambrian gas reservoirs in Anyue gasfield. Petroleum Research. 3, 221–238. https://doi.org/10.1016/j.ptlrs.2018.06.009.

You, X.L., Sun, S., Zhu, J.Q., 2014. Significance of fossilized microbes from the Cambrian stromatolites in the Tarim Basin. Northwest China. Science China Earth Sciences. 57, 2901–2913. https://doi.org/10.1007/s11430-014-4935-z.

Yuan, H.F., 2008. The mechanism of hydrocarbon accumulation, Sinian-Lower Palaeozoic, Sichuan Basin. Chengdu University of Technology. Doctor's thesis.

Yuan, H.F., Liu, Y., Xu, F.H., Wang, G.Z., Xu, G.S., 2014. The fluid charge and hydrocarbon accumulation, Sinian reservoir, Anpingdian-Gaoshiti Structure. Central Sichuan Basin. Acta Petrologica Sinica. 30, 727–736 in Chinese.

Zempolich, W.G., Wilkinson, B.H., Lohmann, K.C., 1988. Diagenesis of Late Proterozoic carbonates: The beck spring dolomite of eastern California. J. Sediment. Res. 58, 656–672. https://doi.org/10.1306/212F8E18-2B24-11D7-8648000102C1865D.

Zenger, D.H., 1983. Burial dolomitization in the Lost Burro Formation (Devonian), east-central California, and the significance of late diagenetic dolomitization. Geology 11, 519–522. https://doi.org/10.1130/0091-7613(1983)11<519:BDITLB>2.0.CO;2.

Zhang, J., Jones, B., Zhang, J.Y., 2014a. Crystals structure of replacement dolomite with different buried depths and its significance to study of dolomite reservoir. China Petroleum Exploration. 19, 21–28 in Chinese.

Zhang, G.Y., Ma, F., Liang, Y.B., Zhao, Z., Qin, Y.Q., Liu, X.B., Zhang, K.B., Ke, W.L., 2015. Domain and theory-technology progress of global deep oil & gas exploration. Acta Pet. Sin. 36, 1156–1166 in Chinese.

Zhang, J., Zhang, B.M., Shan, X.Q., 2014b. Controlling effects of paleo-climate and paleo-ocean on formation of carbonate reservoirs. Pet. Explor. Dev. 41, 135–143. https://doi.org/10.1016/S1876-3804(14)60016-1.

Zhao, W.Z., Hu, S.Y., Liu, W., Wang, T.S., Li, Y.X., 2014. Petroleum geological features and exploration prospect of deep marine carbonate rocks in China onshore: A further discussion. Nat. Gas Ind. 1, 14–23. https://doi.org/10.1016/j.ngib.2014.10.002.

Zhao, D.F., Tan, X.C., Hu, G., Wang, L.C., Wang, X.F., Qiao, Z.F., Luo, S.C., Tang, H., 2021. Characteristics and primary mineralogy of fibrous marine dolomite cements in the end–Ediacaran Dengying Formation, South China: Implications for aragonite-dolomite seas. Palaeogeogr. Palaeoclimatol. Palaeoecol. 581, 110635 https://doi.org/10.1016/j.palaeo.2021.110635.

Zhao, W.Z., Wang, X.F., Wang, X., Wang, K., Shen, A.J., 2022. Stratigraphic sequence re-determination and lithofacies palaeogeographical characteristics of the Sinian Dengying Formation in Sichuan Basin. J. Palaeogeogr. 24, 852–870 in Chinese.

Zhou, Y., Yang, F.L., Ji, Y.L., Zhou, X.F., Zhang, C.H., 2020. Characteristics and controlling factors of dolomite karst reservoirs of the Sinian Dengying Formation, central Sichuan Basin, southwestern China. Precambr. Res. 343, 105708 https://doi.org/10.1016/j.precamres.2020.105708.

Zhu, G.Y., Wang, T.S., Xie, Z.Y., Xie, B.H., Liu, K.Y., 2015. Giant gas discovery in the Precambrian deeply buried reservoirs in the Sichuan Basin, China: implications for gas exploration in old cratonic basins. Precambr. Res. 262, 45–66. https://doi.org/10.1016/j.precamres.2015.02.023.

Zou, C.N., Yang, Z., Dai, J.X., Dong, D.Z., Zhang, B.M., Wang, Y.M., Deng, S.H., Huang, J. L., Liu, K.Y., Yang, C., Wei, G.Q., Pan, S.Q., 2015. The characteristics and significance of conventional and unconventional Sinian-Silurian gas systems in the Sichuan Basin, central China. Mar. Pet. Geol. 64, 386–402. https://doi.org/10.1016/j.marpetgeo.2015.03.005.